https://doi.org/10.5194/egusphere-2024-3687
Preprint. Discussion started: 6 December 2024

Sea ice and mixed layer depth influence on nitrate depletion and associated isotopic effects in the Drake Passage – Weddell Sea region, Southern Ocean

Aymeric P. M. Servettaz[1,2,*], Yuta Isaji[1], Chisato Yoshikawa[1], Yanghee Jang[3], Boo-Keun Khim[4,*], Yeongjun Ryu[5], Daniel M. Sigman[5], Nanako O. Ogawa[1], Francisco J. Jiménez-Espejo[1,6], Naohiko Ohkouchi[1]

[1]Biogeochemistry Research Center, Japan Agency for Marine-Earth Science and Technology, Yokosuka, 237-0061 Kanagawa, Japan
[2]Institute of Arctic Climate and Environment Research, Japan Agency for Marine-Earth Science and Technology, Yokosuka, 237-0061 Kanagawa, Japan
[3]Marine Radioactive Monitoring Group, Marine Environment Research Institute, Korea Marine Environment Management Corporation, Busan 49111, Korea
[4]Department of Oceanography and Marine Research Institute, Pusan National University, Busan 46241, Korea
[5]Department of Geosciences, Princeton University, Princeton, New Jersey 08544, United States of America
[6]Instituto Andaluz de Ciencias de la Tierra, Spanish Research Council, 18100 Armilla, Granada, Spain
[*]*Correspondence should be addressed to*: A.P.M Servettaz (servettaza@jamstec.go.jp) and B.-K. Khim (bkkhim@pusan.ac.kr)

Abstract. The regions near the Antarctic Peninsula in the Southern Ocean are highly productive, with notable phytoplanktonic blooms in the ice-free season. The primary productivity is sustained by the supply of nutrients from convective mixing with nitrate-rich subsurface waters, which promotes rapid phytoplankton growth as the sea ice melts in spring and summer. Surface waters are marked by the contrast between the warmer Drake Passage and the colder Weddell Sea, and seasonal duration of sea ice cover varies accordingly. Sea ice exerts multiple controls over primary production, by shading the light entering the ocean and stratifying the upper ocean with freshening by ice melt. However, the interaction between sea ice and productivity remains poorly characterized because satellites are unable to quantify biomass in partially ice-covered ocean, and direct measurements are too scarce to characterize the seasonally varying productivity. Here we evaluate productivity by assessing removal of nitrate from surface waters by biological nutrient utilization, and study the associated change in $\delta^{15}N$ of nitrate. We use a combination of bottle samples and *in situ* nitrate measurements from published databases, completed by two transects with isotopic measurements. The timing of sea ice melt date conditions the initiation of nitrate drawdown, but the annual minimum of nitrate only weakly correlates with sea ice concentration. As previously reported, we observe that $\delta^{15}N$ of nitrate increases with nitrate depletion. Interestingly, the lowest nitrate depletion and $\delta^{15}N$ values are found in the central region of N-S transects, where intermediate temperature and sea ice conditions prevail. Deeper mixing in waters that passed through the northern Bransfield Strait may explain higher nitrate concentration due to both a greater nitrate resupply and reduced productivity under light limitation in deeply mixed waters, confirmed by isotopic fractionation effects during nitrate uptake and nitrogen isotope modelling. This highlights the importance of oceanographic controls on productivity patterns in sea-iced regions in the Southern Ocean.

1. Introduction

In the Southern Ocean (SO), phytoplanktonic blooms develop near the Antarctic continent, in the seasonally ice-covered region and in coastal polynyas (Soppa et al., 2016). The marginal ice zone, where sea ice is present but scattered, contributes to a large part of SO productivity (Arrigo et al., 1998; Savidge et al., 1996). Coastal regions around the Antarctic Peninsula are particularly productive as apparent from satellite-based ocean color scanning (Arrigo et al., 2008; Moreau et al., 2020), which stands out from the low-chlorophyll and high-nutrients waters that characterize most of the SO. Oceanic regions south of the Polar Front play an important role in carbon sequestration, due to the high efficiency of carbon export in areas of deepwater formation (DeVries et al., 2012; Gruber et al., 2009; Huang and Fassbender, 2024; Sabine et al., 2004; Wang et al., 2023). Understanding productivity patterns and limitations in the seasonally ice-covered SO is thus an important aspect of the global climate.

The Antarctic Peninsula and surrounding oceans constitute one of the fastest warming regions in the Southern Hemisphere (Fan et al., 2014; Jones et al., 2016), and yet challenges remain to understand how primary productivity will react to such warming. Although increase of surface water chlorophyll concentration may hint towards increased open-water productivity (Moreau et al., 2015), this method does not account for productivity within the marginal ice zone and may primarily reflect the shift from marginal ice zone productivity to open-water productivity due to longer ice-free season. The presence of sea ice prevents the estimation of chlorophyll concentration from satellites, hampering our ability to remotely evaluate the productivity of seasonally ice-covered regions (Bélanger et al., 2007). While *in situ* quantification of chlorophyll concentration may be useful to estimate biomass of primary producers, it only provides information at a given date, and because such measurements are rarely repeated throughout a growth season, they cannot be used to quantify seasonal productivity and export. Indeed, blooming phases in the SO are marked by a high renewal rate of phytoplankton, with turnover rate of phytoplankton reaching 1 day^{-1} (Arteaga et al., 2020). Alternative productivity estimates have been proposed, relying on the quantification of nutrient uptake by primary producers to estimate production and export in the SO (Moreau et al., 2020). This quantification relies on the seasonal dynamics of nutrient resupply: deep mixing in winter replenishes the nutrient pool, whereas surface stratification during productive season limits exchanges with underlying water, creating a nutrient budget that will be consumed by primary producers (Codispoti et al., 2013). This method does not account for regenerated nutrients within the surface layer by heterotrophic activity during growth season (Fripiat et al., 2015), but is useful to quantify the seasonal export of organic matter as sinking particles (Flynn et al., 2021; Mdutyana et al., 2020).

In the SO, upwelling of nutrient-rich Circumpolar Deep Water at the Antarctic divergence supplies substantial amount of nitrate and phosphate, so phytoplanktonic growth may rather be limited by iron and silicate (M. Franck et al., 2000; Moore et al., 2002). In the coastal regions around the Antarctic Peninsula and nearby islands, dissolved iron is abundantly supplied by desorption from sediment on the shelves or the coasts, glacier melt, and dust deposition (Ardelan et al., 2010; Jiang et al., 2019; Sherrell et al., 2018). Therefore, contrary to the largest part of the SO, iron is not the limiting factor on phytoplanktonic growth in coastal areas such as in the Bransfield Strait (hereafter abbreviated BS, Frants et al., 2013; Measures et al., 2013). Rather, light availability, controlled by ice shading and vertical mixing, limits phytoplankton growth in these areas (Gonçalves-Araujo et al., 2015), which is especially true for winter when light intensity is low (Hatta et al., 2013).

Sea ice has two opposite effects on light availability: ice shades underlying water when it is present, but its melting releases buoyant freshwater that stabilizes the density structure of upper water column and maintains phytoplankton community in euphotic zone (Taylor et al., 2013). We thus hypothesize that sea ice melt contributes to thinning the mixed layer above which the water is actively mixed by winds. Besides, in areas of sea ice formation, brine rejection favorizes winter convective mixing and nutrient influx from nitrate-rich subsurface waters. This replenishes surface water nutrients, which may then be used next growing season by primary producers. While some algae also develop within brines and pools of sea ice, their contribution to seasonal biomass productivity is relatively small (Arrigo, 2017). Due to its complexity and opposite effects, the influence of sea ice on seasonally integrated phytoplankton productivity remains poorly characterized.

Nitrate is a major source of nitrogen for microorganisms (Ohkouchi and Takano, 2014), with additional variable contributions of nitrite, ammonium, and urea throughout the season (Goeyens et al., 1995; Mengesha et al., 1998). While N_2 fixation can be an alternative nitrogen source in oligotrophic subtropical seas, this contribution is negligible in the SO (Zehr and Capone, 2021). In winter between the ice edge and the Polar Front, nitrification is an important source of regenerated nitrate (Smart et al., 2015), causing the net primary productivity and net nitrogen uptake to be decoupled (Mdutyana et al., 2020). In summer, however, primary productivity is primarily supported by nitrate both in the ice-free SO (Mdutyana et al., 2020) and the seasonally ice-covered zone (DiFiore et al., 2009). In the Weddell Sea (WS), where sea ice concentration (SIC) is usually high, nitrification is slower, suggesting that nitrate utilization may reflect directly net primary productivity (Flynn et al., 2021). Quantifying nitrate depletion in surface water can therefore be used to estimate productivity in summer, or at least organic matter exported to deeper waters.

In this study, we explore the relationship between nitrate concentration and sea ice characteristics in the SO near the tip of the Antarctic Peninsula, to clarify the impact of sea ice on phytoplankton productivity. We first compare satellite-derived estimations of SIC by area, available year-round, to numerous nutrient concentration that has been widely

https://doi.org/10.5194/egusphere-2024-3687
Preprint. Discussion started: 6 December 2024

measured in the SO both with regular sampling (Olsen et al., 2016) and automated *in situ* quantification (Johnson et al., 2017). We also describe in further detail a transect of nitrate concentration and its nitrogen isotope, which is expected to record isotopic effects during nitrate consumption by primary producers (DiFiore et al., 2009; Sigman et al., 1999). The summarized data is then explained with an isotope-enabled ecosystem model.

2. Oceanographic setting

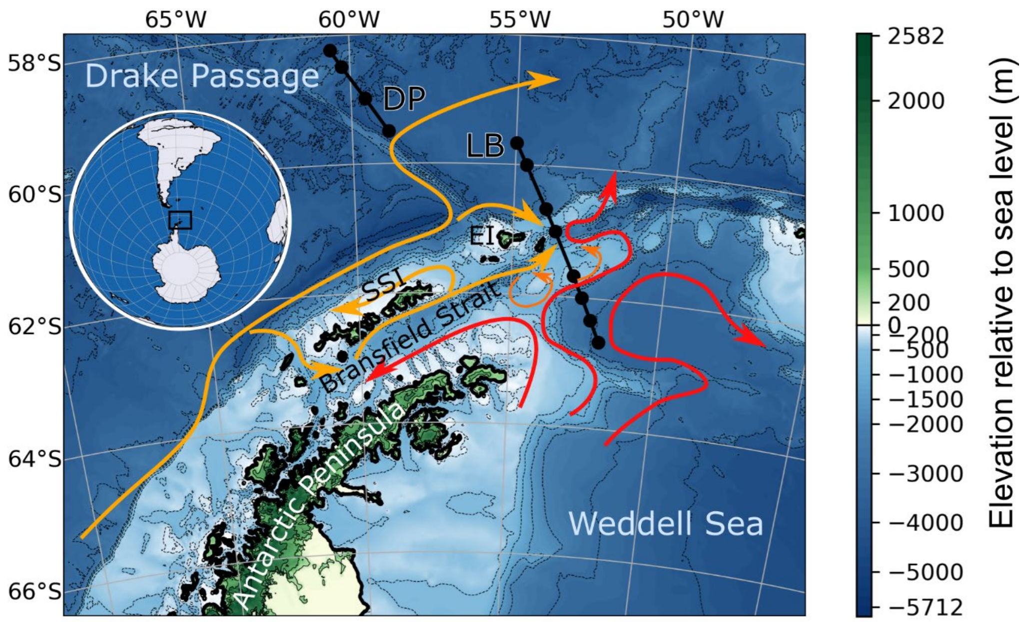

Figure 1. Regional map of the northern Antarctic Peninsula, Bransfield Strait, South Shetland Islands (SSI), Elephant Island (EI), and parts of the Weddell Sea and Drake Passage. Arrows highlight the surface water circulation, orange for water originating from the west side, and red for water exiting the Weddell Gyre (Moffat and Meredith, 2018; Thompson et al., 2009). DP and LB refer to two transects discussed in Sect. 4.1; black dots represent the location of bottle sampling stations. Elevation from ETOPO 2022 (NOAA, 2022).

North of the Antarctic Peninsula, two surface water masses with distinct properties converge in the BS (Fig. 1; Sangrà et al., 2011). Transitional Zonal Water with Weddell Sea influence (TWW) enters BS from the southeast via the westward coastal current, running along the tip of the Antarctic Peninsula. In the northwest of the BS, Transitional Zonal Water with Bellingshausen influence (TBW) enters via a branching derived from the Antarctic Circumpolar Current, and flows northeastward in the Bransfield Current along the South Shetland Islands (SSI). Further east, this current divides into a return current north of SSI (Moffat and Meredith, 2018) and an eastward branch passing south of Elephant Island (Gordon et al., 2000; Thompson et al., 2009). TBW and TWW are separated by a front with a surface gradient of temperature extending to 50-100 m depth, the Peninsula Front, and subsurface gradient, the Bransfield Front, located further north beneath the Bransfield Current jet at depths of 150 to 500 m (Sangrà et al., 2011). The Bransfield Current is associated with TWB-containing anticyclonic eddies in the upper 80 m at its southern boundary (Thompson et al., 2009). The colder TWW supports the persistence of sea ice for a longer part of the year in the southeast of the Antarctic Peninsula (Fig. 2). Relative contribution of these two surface water masses to BS, and the position of the front separating them, has been suspected to vary with westerly wind intensity (Vorrath et al., 2020). The water masses properties condition the development of primary producers. Previous studies have found higher concentration of chlorophyll in the TWB, that was interpreted as warm waters with a shallow pycnocline being more productive (Gonçalves-Araujo et al., 2015; La et al., 2019; Pereira Granja Russo et al., 2018).

https://doi.org/10.5194/egusphere-2024-3687
Preprint. Discussion started: 6 December 2024

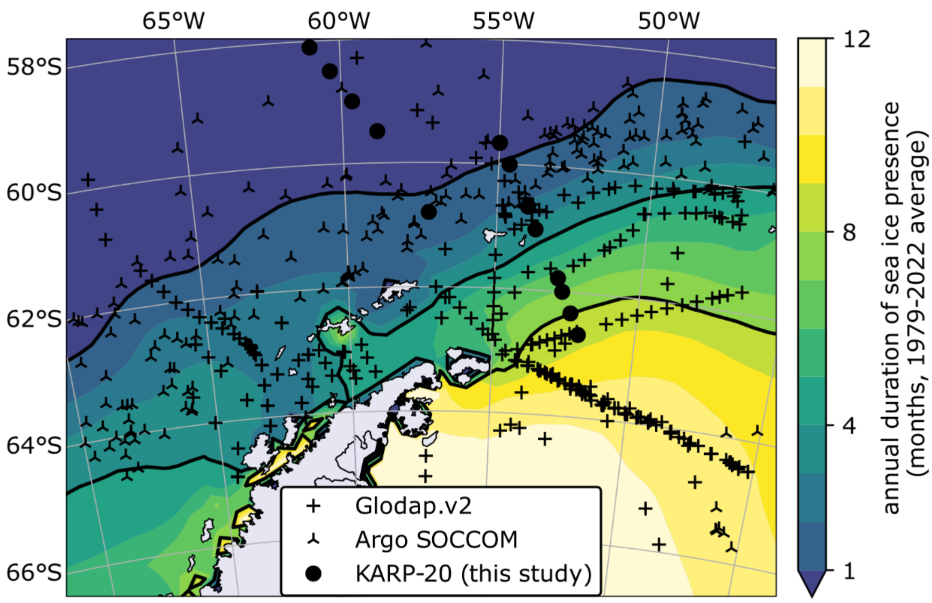

Figure 2. Map of sea ice seasonality in the Southern Ocean and nitrate data location. Duration of sea ice presence in months per year, defined as the number of months where sea ice concentration is greater than 15% by area (color scale, with black contour lines at 1, 4, and 8 months). Sea ice in coastal areas is reportedly inaccurate due to the coarse resolution of the sensor (Lavergne 2023). Symbols indicate the location of nitrate concentration data used in this study, classified by data source.

3. Material and methods

A large number of measurements have been made publicly available in recent years through data repositories. We briefly describe the datasets used, and additional original data presented in this study. We use a regional subsection of the datasets around the Antarctic Peninsula (Fig. 2).

3.1 KARP-20 Nitrate concentrations and isotopes

The Korea Antarctic Research Program 20th expedition (KARP-20) conducted Conductivity-Temperature-Depth (CTD) profile using SBE CTD 911plus along three transects in the DP region between the 1st and the 31st of December 2006. Water bottle samples were collected for nitrate analysis at 13 stations (black circles on Fig. 2) with 12 water depth sampled at each location. Salinity and temperature from CTD were used to determine the potential density anomaly, σ_0.

Nitrate concentration of each bottle was determined after reduction of nitrate and nitrite to nitric oxide using a V(III) reagent, then quantified by chemiluminescence (Braman and Hendrix, 1989). Our concentration measurements include nitrite, whose contribution is expected to be small in the SO in summer (Thomas et al., 2024). In addition to nitrate concentration, $\delta^{15}N$ of nitrates were analyzed using the "denitrifier method", where nitrate is converted to nitrous oxide gas by modified denitrifying bacteria lacking nitrous oxide reductase activity (Sigman et al., 2001). After transformation of nitrate to nitrous oxide, the nitrogen isotopic composition of resulting nitrous oxide is analyzed with gas chromatography-isotope ratio mass spectrometry (GC-IRMS) at Princeton University (USA).

3.2 Glodapv2 nitrate concentrations

The Global Ocean Data Analysis Project Version 2 (GLODAPv2; Olsen et al., 2016) is a collection of biogeochemical bottle data, extending from the World Ocean Circulation Experiment database with quality-controlled additions from more recent cruises. A thorough description of the GLODAPv2.2022 used here is given by Lauvset et al. (2022).

Nitrate concentrations in bottle samples are typically determined using the colorimetric absorbance measurement after reduction to nitrite (Armstrong et al., 1967). Measurements included in GLODAPv2 database were quality checked and outliers are removed from the published dataset (Key et al., 2015). Here we only briefly describe how we selected samples used in our study. We defined a regional subset around the Antarctic Peninsula with 45 °W–78 °W and 56 °S–66 °S boundaries, and selected stations where sea ice was present in the year prior to sampling, thus excluding the permanently open ocean zone (see Sect. 3.5 for sea ice data used). Bottles included in this subset were collected between September 1989 and January 2016. In addition to the nitrate value, we use the potential density anomaly (σ_0) for definition of mixed layer depth (MLD). In the subregion defined for the present study, a total of 187 stations with at least one nitrate measurement above MLD were used (the calculation of MLD used here is given in Section 3.4). While nitrate concentration measurements are very precise with around 0.2% uncertainty, comparison of deep bottles (>1000 m) with nearby (<250 km) measurements give variations usually lower than 2% of the measured value (Aoyama, 2020), which can provide a base estimate of consistency of repeat nitrate measurements, and adjustment were made in GLODAPv2 which resulted in a similar consistency level (Lauvset et al., 2022), even if it is not uncertainty in the strict sense.

3.3 SOCCOM Argo floats *in situ* nitrate estimation

Recent developments of ultraviolet spectrophotometers nitrate sensors provide *in situ* quantification of nitrate concentrations using its absorbance in the ultraviolet band, without requiring chemical transformation (Johnson et al., 2013; Johnson and Coletti, 2002; MacIntyre et al., 2009). When mounted on profiling floats, they can profile the nitrate content of the water column, and are set to measure 300 profiles at a rate of one profile every ~5 days which can make the battery last for a couple of years (Johnson et al., 2013). The SO Carbon and Climate Observations and Modeling (SOCCOM) has deployed 295 floats in the SO, equipped with biogeochemistry sensors including submersible nitrate sensor (as of May 2024. source: https://www3.mbari.org/soccom/tables/SOCCOM_float_performance.html). A description and evaluation of accuracy of nitrate sensors used on SOCCOM floats is given in Wanninkhof et al. (2016). We use a quality-controlled dataset where nitrate sensors were calibrated prior to deployment, and offset and drift were adjusted throughout the float service time using known concentration at depths below 1000 m as a reference for calibration (Maurer et al., 2021). This lowers the uncertainty on nitrate concentrations to 0.5 µmol kg^{-1}. SOCCOM floats have previously been used to assess nitrate drawdown and net community production (Johnson et al., 2017), and hereafter we specifically assess the influence of sea ice on nitrate drawdown. We use a total of 194 profiles from 16 floats, all measured in the regional subset previously defined, dated between January 2016 and June 2022.

3.4 Definition of mixed layer depth and surface nitrate depletion

The surface mixed layer depicts a layer actively mixed by wind activity, leading to homogenous physical and chemical properties. Its depth is controlled by the strength of winds and the density gradients, such as a change of temperature or an increase of density indicates the MLD. In the SO, it is preferable to use a density criterion due to the low temperatures throughout the year and significant contribution of meltwater to salinity changes. Therefore, we define the MLD as the depth with a density increased by $\Delta\sigma = 0.03$ kg m^{-3} relative to the reference density taken at 10-m depth (de Boyer Montégut et al., 2004).

Surface nitrate concentrations presented in this study are an average of all available measurement points in the mixed layer. For summer samples, we also use nitrate depletion, defined as the difference in nitrate concentration between the surface mixed layer and a subsurface water referred to as Winter Water (WW; Goeyens et al., 1995). WW describes water that was last mixed during the previous winter, when cold surface temperature leads to higher density, thereby increasing the depth of mixing. Similarly to Flynn et al. (2021), we define the WW layer as the layer between the MLD and the depth of the temperature minimum within 20 to 200 m below the MLD. WW serves as a reference for ocean conditions before the seasonal growth of phytoplankton, therefore nitrate depletion is defined as the difference between nitrate concentration in the WW (average of all measurements in the depth range) minus surface nitrate concentration.

Input of meltwater from sea ice with low nitrate concentration could bias this depletion value due to the dilution of nitrate in surface waters. We corrected for this dilution effect following the method of Flynn et al. (2021), proposed for the WS. To evaluate the maximum dilution potential, we also use the minimal value for nitrate concentration in sea ice of 1 µmol kg^{-1} reported for the Bellingshausen and Weddell Seas (Fripiat et al., 2014). Note that, as in the original study by Flynn et al. (2021), this correction only marginally affects the depletion values; in the samples considered here, the average summer salinity decrease is 0.18 PSU (1^{st} decile – 9^{th} decile range: 0.04–0.36 PSU), and result in an average dilution correction of 0.18 µMol kg^{-1} (1^{st} decile – 9^{th} decile range: 0.04–0.37 µmol kg^{-1}) for nitrate depletions. The slightly greater dilution effect for strong salinity decrease is due to the higher seawater nitrate concentration with high sea ice meltwater contribution. Therefore, the interpretations that we would make in this article do not differ. We hereafter refer to meltwater-dilution corrected nitrate depletion as "nitrate depletion (corrected)".

3.5 Sea ice concentration

We use daily SIC retrieved from version 3 of the EUMETSAT Ocean and Sea Ice Satellite Application Facility sea-ice products for the 1979-2022 period (OSI SAF 2022a, 2022b; updated from Lavergne et al., 2019). This 25 km resolution reconstruction is based on microwave emissivity of surface ocean, with SIC calculated from brightness temperature. Accuracy of SIC by area was evaluated to 8 % in version 2 of this dataset (Lavergne et al. 2019). Updated processing chain and auxiliary climate fields in version 3 used here result in a reduced bias (Lavergne et al., 2023).

For each nitrate concentration measurement, we extracted the SIC on the grid cell corresponding to measurement location, at daily resolution on the year preceding the measurement date. We therefore retrieve the sea ice condition in the time leading up to nitrate measurement. This approach enables monitoring the anomalies in SIC on the year of measurement, since sea ice conditions at the measurement location may substantially differ from average due to the high international variability (Parkinson and Cavalieri, 2012; Wang and Wu, 2021).

3.6 Nitrogen isotope modelling

We simulated the nitrogen cycle in the surface ocean using an isotope enabled ecosystem model. This model has six compartments, phytoplankton (PHY), zooplankton (ZOO), particulate organic nitrogen (PON), dissolved organic nitrogen (DON), nitrate (NO_3^-), and ammonium (NH_4^+). The prognostic variables are the N and ^{15}N concentrations. The equations and parameters excluding nitrification are the same as those used by Yoshikawa et al., (2005), which successfully simulated nitrogen isotope observations in the Sea of Okhotsk, a high-latitude marginal sea. The equations and parameters for nitrification are the same as those used by Yoshikawa et al. (2022), which includes photoinhibition terms. The nitrogen isotope fractionation parameters are the same as those used by Yoshikawa et al. (2024).

We applied the model to the ocean environment in three locations around the Antarctic Peninsula: Drake Passage (DP: 60 °S, 60 °W), Eastern Bransfield Strait (BS: 62 °S, 55 °W) and Weddell Sea (WS: 64 °S, 50 °W). This model has two vertical layers (surface layer: 0-20 m; subsurface layer: 20-120 m). Light intensity at the surface was taken from long term mean daily net shortwave radiation fluxes of NCEP-NCAR Reanalysis (Kalnay et al., 1996). Water temperature at upper and lower layers and MLD were taken from the World Ocean Atlas 2018 (Garcia et al., 2019). Water exchange between the surface and subsurface layers, and between the subsurface layer and the layer deeper than 120 m are changed seasonally in conjunction with the MLD. Boundary conditions at 120 m depth for the nitrate concentration were taken from the World Ocean Atlas 2018 (Garcia et al., 2019) and its $\delta^{15}N$ value was fixed to 5‰ which is in the range of the observations at 120 m during KARP-20 (Sect. 4.2). The model was integrated for a 4-year spin-up period, and then used to simulate a period of 1 year.

4. Results and Discussion

4.1 Sea ice impact on nitrate depletion

In this section we assess the impact of sea ice on nitrate depletion, to verify the hypothesis that large seasonal variations in sea ice could contribute to stratification of the surface water, as sea ice retreat enhances light availability and nutrient consumption by primary producers (Sallée et al., 2010) while reducing the available nutrient pool due to the thinning of the surface mixed layer (Smith, and Nelson, 1986; Taylor et al., 2013).

https://doi.org/10.5194/egusphere-2024-3687
Preprint. Discussion started: 6 December 2024

We use the sea ice seasonality at the location where the nitrate concentration was measured. We did not backtrack the water parcel or the sea ice. Also, we assume that sea ice seasonality at the point of nitrate measurement is similar to that of the water parcel present at the time of nitrate sampling, *i.e.* not resolving the effects of ocean circulation or drifted ice over the course of a season. A parcel-tracking approach would be technically possible using coupled ocean-sea ice model, but we do not expect significant improvement of our results due to limitations in modelled ice drift (Uotila et al., 2014).

4.1.1 Spatial patterns

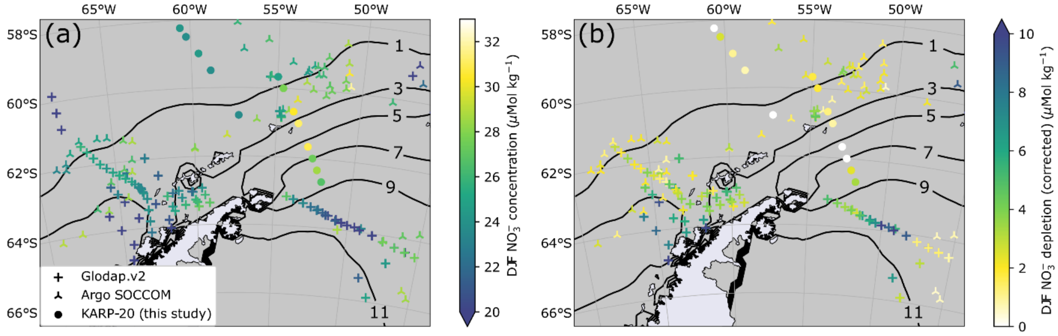

Figure 3. (a) Map of summer surface water nitrate concentration (color scale) classified by data source (symbol type). Contour lines indicate the 1979-2022 average sea ice presence duration in months per year. (b) same as (a), but for summer nitrate depletion (corrected). The definition of summer depletion and its correction are given in Sect. 3.4. The lower number of points for nitrate depletion results from the absence of nitrate concentration data in the subsurface layer of winter water.

Spatial patterns of summer (December, January, and February: DJF) nitrate concentration (Fig. 3a) and depletion (Fig. 3b) do not particularly match the sea ice presence gradient (Fig. 2). Nitrate depletion is intense in the western BS and Gerlache Strait, with values consistently exceeding 5 µmol kg^{-1}, as described by Castro et al. (2002) which first described this data included in Glodap.v2. They attributed this strong depletion to thriving phytoplankton blooms in the very stable surface waters. In addition, strong depletion values close to 10 µmol kg^{-1} are observed in the WS around 50 °W, contrasting with lower depletion values further east, of profiles on the same cruise (Fahrbach, 1993). KARP-20 nitrate concentrations east of Elephant Island (61 °S, 54 °W to 62 °S, 52 °W) are among the highest nitrate concentrations measured for summertime, with values exceeding 30 µmol kg^{-1}. KARP-20 stations also reveal that nitrate is not depleted relative to subsurface waters in the outlet of the BS (discussed in further detail in Sect. 4.1). Generally, nitrate concentration or depletion do not correspond spatially to sea ice duration (Fig. 2).

4.1.2 Timing of ice melt

The biological activity in the SO is restricted in the austral spring by light, both from low incident light angle and from the shading effect of remaining sea ice. Near the Antarctic Peninsula, the duration of sea ice cover varies latitudinally from the quasi-permanently ice-covered WS to the open ocean in the center of DP (Fig. 2). As the sea ice retreats, the light limitation is expected to be reduced, and the water column is stabilized by release of low-density meltwater (Taylor et al., 2013). This would favor phytoplanktonic growth and nitrate consumption.

To visualize the effect of ice retreat on nutrient drawdown, we show how nitrate depletion (surface minus subsurface concentration, see Sect. 3.4) varies during the season, and relative to the day of ice melt at different locations around the Antarctic Peninsula (Fig. 4). In September and October, the surface nitrate depletion is minimal, owing to deep mixing and limited nitrate utilization. In late spring to early summer (November-December), the surface nitrate is more depleted, although approximately half of the waters sampled during these months have nitrate depletion of less than 3 µmol kg^{-1}. In January and February, the surface nitrate is depleted by more than 5 µmol kg^{-1} at most sampling stations. Nitrate depletion exceeding 5 µmol kg^{-1} is encountered throughout the summer. In March, the deepening of

https://doi.org/10.5194/egusphere-2024-3687
Preprint. Discussion started: 6 December 2024

MLD vertically homogenizes the nitrate concentrations, and in conjunction with the slowing of biological uptake in autumn, the nitrate depletion in surface water decreases.

Timing of ice melt controls the initiation of phytoplankton bloom and associated nutrient uptake through the formation of buoyant surface meltwater (Fig. 4). Although few samples were recovered prior to complete ice melt, the nitrate concentrations measured before ice melt are marginally depleted relative to subsurface waters, with less than 5 µmol kg^{-1} difference. The highest of these pre-ice melt depletions comes from the profiles measured in July when the water column may not have been homogenized, and the depletion is probably a remnant of the previous year. Low nitrate depletions prior to ice melt results from the low biological activity, the larger nutrient resupply due to non-segregated surface waters, or a combination of both. After sea ice melts, depletion greater than 5 µmol kg^{-1} is frequent, but not observed in all samples. More than half of nitrate depletion values are still lower than 5 µmol kg^{-1}. Although there is a large spread of nitrate depletion values at any time after the ice melt, the highest depletions are reached after about 50 days, which may reflect the entire duration of the phytoplankton bloom following ice melt, with the lowest nutrient values after the bloom phase ends (Arteaga et al., 2020, and supplement therein). Later in the season, phytoplankton growth slows down (Arteaga et al., 2020), and the relative contribution of regenerated nutrients to biological production increases (decrease in the *f*-ratio, Fripiat et al., 2015; Mdutyana et al., 2020). Additionally, weakening of the stratification in later season can lead to decrease in surface nitrate depletion, as mixed layer gradually deepens and incorporates nitrate-rich water from the subsurface.

In summary, nitrate depletion is strongest when the sea ice melting precedes light maximum by about 50 days (Fig. 4a). It points out the high nutrient utilization in well-lit buoyant lens of meltwater, supporting the hypothesis of sea ice control on nutrient utilization. However, the large variability of nitrate depletion noted at any point in time indicates that while nutrient utilization may be optimal at a certain timing after ice melts, nutrient depletion will not necessarily occur at this time. Three-season monitoring near Palmer Station suggests that stratification by surface temperature increase after sea ice has melted is the main condition for bloom initiation (Moline and Prézelin, 1996), which can explain the equivocal relationship between sea ice retreat and bloom initiation: temperature remains low as long as sea ice remains, but sea ice melt is not necessarily immediately followed by a temperature increase. Temperature rise may trigger the bloom initiation at a delay with ice melt by enhancing both stratification and productivity.

https://doi.org/10.5194/egusphere-2024-3687
Preprint. Discussion started: 6 December 2024

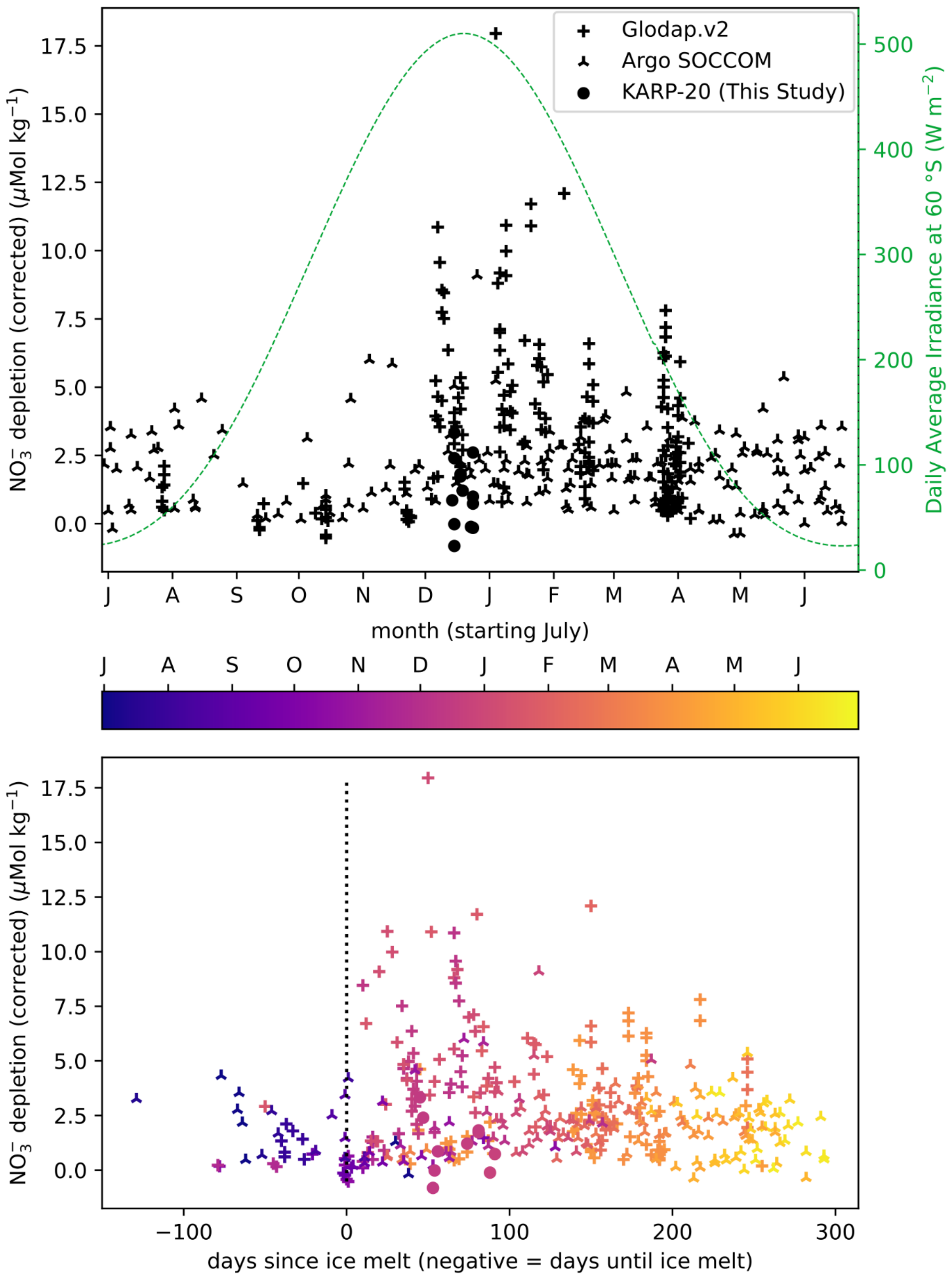

303

304 **Figure 4. Nitrate depletion as a function of day of year (a) and day since ice melt (b). The annual cycle of insolation is given**
305 **as daily average irradiance at the top of atmosphere at 60 °S (green dashed line). The color of points in (b) indicates the**
306 **timing in the year.**

307 ### 4.1.3 Seasonal range of ice concentration

https://doi.org/10.5194/egusphere-2024-3687
Preprint. Discussion started: 6 December 2024

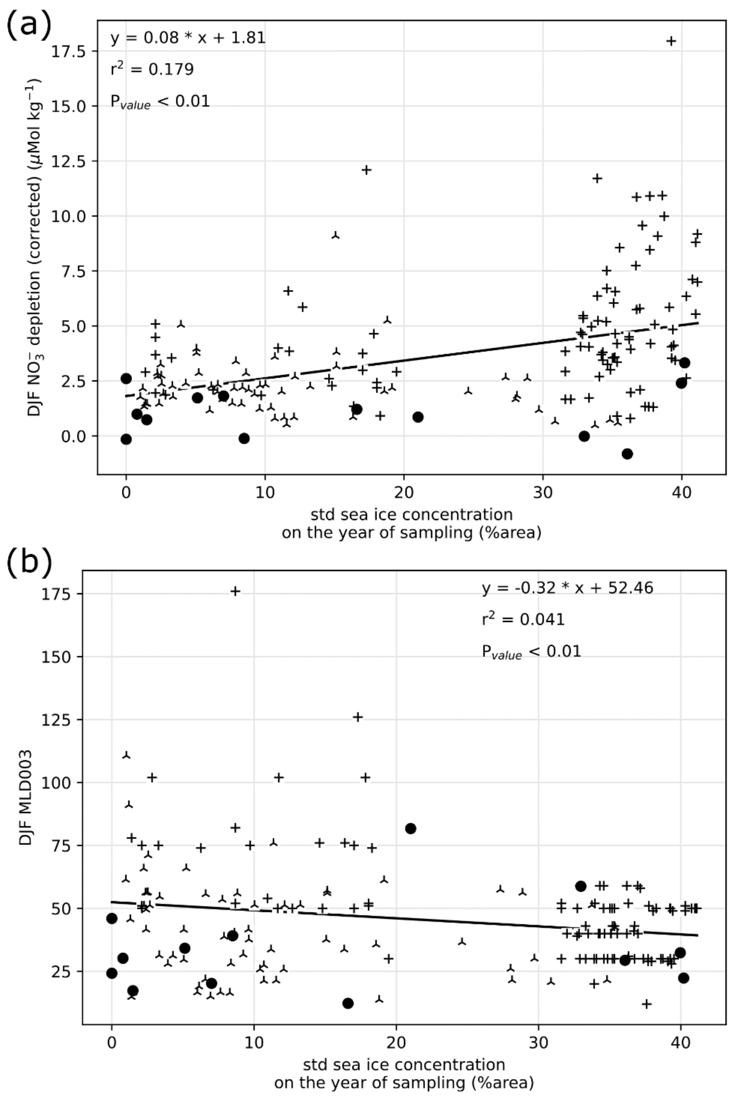

Figure 5. (a) Summer (December, January, and February: DJF) nitrate depletion as a function of sea ice seasonal range estimated with yearly standard deviation of sea ice concentration. (b) summer (DJF) mixed layer depth (MLD) as a function of sea ice seasonal range. Data source is indicated by symbols, consistently with previous figures.

In this section we investigate whether an increased seasonal variation of the SIC (area covered) would favor nitrate depletion, through the shoaling of the MLD which improves the light availability while reducing the amount of nutrients. Although volume or mass of sea ice would be more suited for this comparison, parameters relying on thickness are poorly constrained in the SO (Kwok and Kacimi, 2018; Williams et al., 2015). We thus rely on satellite data to estimate the area of sea ice coverage. We use standard deviation of SIC (SD_{sic}) over the year leading up to the sampling to evaluate the range of seasonal changes in sea ice cover. It is preferred over average sea ice to rule out high sea ice cover grid points such as in the WS, where SIC is high year-round, leading to high average and low variability sea ice cover.

https://doi.org/10.5194/egusphere-2024-3687
Preprint. Discussion started: 6 December 2024

Summer nitrate depletion varies widely at the regional scale studied here, with values ranging from 0 up to 12.5 µmol kg^{-1}. While most nitrate depletion greater than 5 µmol kg^{-1} occurs at SD_{sic} higher than 10%, there is nevertheless a wide range of nitrate depletion encountered at any SD_{SIC} (Fig. 5a). Notably, non-depleted (depletion < 1 µmol kg^{-1}) waters are observed regardless of the SIC. A weak positive correlation ($r^2 = 0.179$, $p_{value} <0.01$) between nitrate depletion and SD_{SIC} suggests that about 18 % of the variability of both sea ice and nitrate depletion is shared. Although we cannot conclude on a causal relationship, changes in SIC may at most be responsible for 18% of the variability in nitrate depletion. This low correlation indicates that seasonal amplitude of sea ice alone cannot explain all the variability found in the surface nitrate depletion in summer.

We also tested if high yearly SIC leads to reduced MLD, through the meltwater supply to the surface (sample locations are mostly ice-free in summer, except for a few locations with partial ice cover). Because we analyze the sea ice seasonality at a fixed location for simplicity, this relies on the assumption that sea ice melts locally, ignoring possible ice drift and/or meltwater horizontal transport. Comparing summer MLD with yearly SIC (Fig. 5b) reveals that while stations with yearly SIC exceeding 20 % have a MLD consistently shallower than 60 m, a wide range of MLD is encountered at stations with low SIC, implying control of MLD by additional factors. Indeed, sea ice melting controls freshwater inputs and salinity, but temperature is also an important factor of stability in the sea ice covered section of the SO (Pellichero et al., 2017). Consequently, despite being significantly correlated ($p_{value} < 0.01$), MLD and SIC only share 5.7 % variability ($r^2 = 0.057$). At the regional scale, sea ice seasonality has a limited influence on MLD. In turn, the summer nitrate depletion is mostly independent of sea ice cover, although it is less frequently depleted in waters with scarce sea ice cover.

Reasons to why sea ice seasonality does not control nitrate depletion at the regional scale likely emerge from the variety of settings across fronts and basins around the Antarctic Peninsula. Light limitation is often indirectly linked to sea ice: the removal of shading is not sufficient to trigger bloom and nutrient drawdown (Fig. 4). It is possible that light limitation is relieved with stratification of the upper ocean layer, which can occur with a delay after ice melts. Density profile and MLD are more likely to be controlled by temperature rather than salinity in the seawaters north of the Peninsula Front (Gonçalves-Araujo et al., 2015), where low inputs of freshwater are compensated by stronger temperature-driven stratification. On the contrary in the WS and southern half of BS, sea ice provides freshwater lowering salinity, but it also buffers the temperature and maintains a cool surface even in the summer.

4.2 Observation and modelling of ^{15}N enrichment

Nitrate uptake by phytoplankton is associated with an increase of $\delta^{15}N$ of the nitrate remaining in seawater (following the δ notation relative to the ratio $^{15}N/^{14}N$ in atmospheric N_2), due to the preferential uptake of ^{14}N by the microorganisms (Sigman et al., 1999). The uptaken nitrate is transformed into organic molecules with an average biosynthetic nitrogen isotope effect ε of around 5‰ (Altabet and Francois, 2001; Sigman et al., 1999; Waser et al., 1998), given by the difference in kinetics of reaction rates between ^{14}N and ^{15}N: $\varepsilon = {}^{14}k/{}^{15}k - 1$. Applied in a Rayleigh distillation, isotope effect can be approximated by:

$$\varepsilon = \frac{\delta^{15}N_{initial} - \delta^{15}N}{\ln(NO_3^-) - \ln\left(NO_3^-{}_{initial}\right)} \tag{1}$$

(Mariotti et al., 1981; Sigman et al., 1999; ε is defined as positive if $\delta^{15}N$ of remaining nitrate increases when nitrate concentration decreases).

This effect may be slightly more positive in light-limited environments (DiFiore et al., 2010; Needoba et al., 2004; Needoba and Harrison, 2004). Consequently, nitrate concentrations are inversely correlated with $\delta^{15}N$ of nitrate in the nutrient-rich SO (Lourey et al., 2003; Sigman et al., 1999). In this section, we focus on the KARP-20 transect, with measurements of nitrate concentration and $\delta^{15}N$, to gain further insights on nitrate uptake. We then evaluate observed trends using a nitrogen cycle isotope model with environmental forcings.

4.2.1 KARP-20 nitrate concentration and $\delta^{15}N$ observations

https://doi.org/10.5194/egusphere-2024-3687
Preprint. Discussion started: 6 December 2024

Here we present the $\delta^{15}N$ of nitrate collected in the DP and BS (location of transects given in Fig. 1) and discuss the environmental factors that can affect nitrate concentration and isotopes. The goal of this section is to confirm that the relationship between nitrate concentration and isotopes is respected in this region, and understand the environmental forcings that control them.

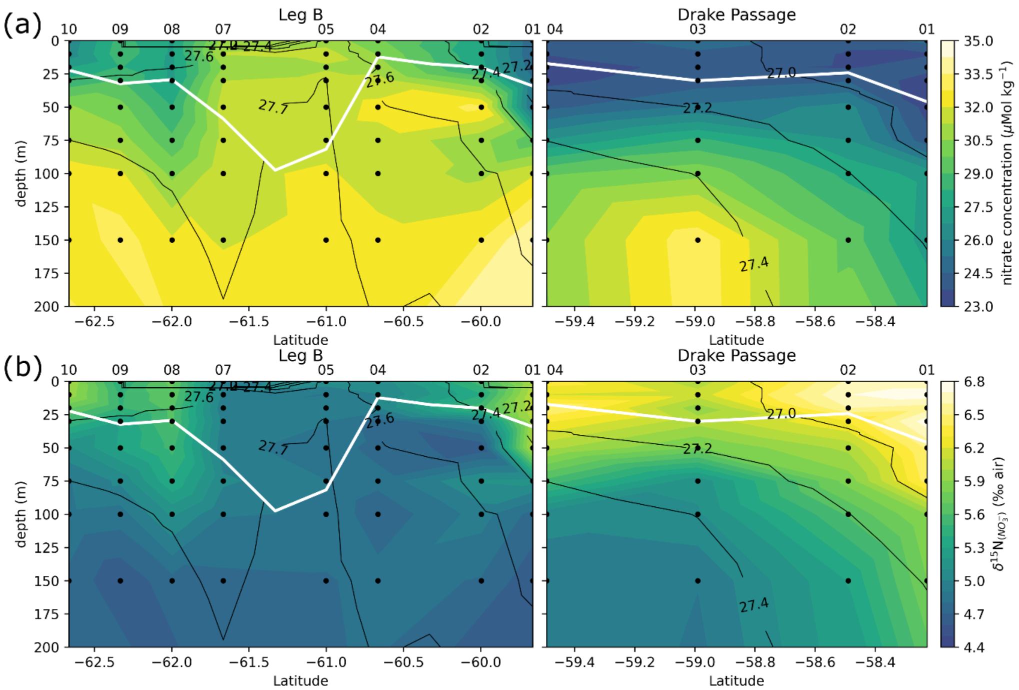

Figure 6. Leg B and Drake Passage Transects, with color shadings of nitrate concentration (a) and $\delta^{15}N$ of nitrate (b). Black contours represent the CTD potential density anomaly (σ_0 in kg m^{-3}). White line highlights the MLD, computed as the depth with a potential density increased by 0.03 kg m^{-3} relative to the density at 10 m depth.

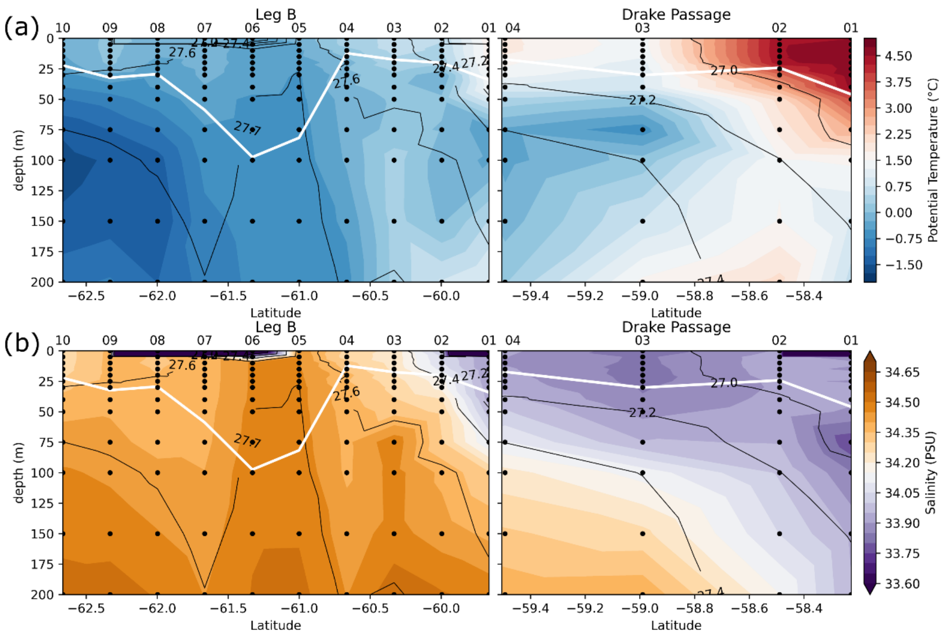

Figure 7. Same as Fig. 6, but for potential temperature (a) and salinity (b).

Transects of nitrate concentration in the DP and eastern BS (Fig. 6a) depict typical SO summer pattern with partial depletion in the surface waters, down to a minimum of 23 µmol kg^{-1} in the DP compared to subsurface waters, where concentrations exceed 31 µmol kg^{-1} (profiles also given in Appendix Fig. A1). Isopycnals follow the general SO pattern with deepening at lower latitudes, except for the center section of LB transect (60.7 °S to 61.7 °S) with a shoaling of the 27.7 kg m^{-3} isopycnal, indicating the presence of high-density water at relatively shallow depth. The high density is due to higher salinity (>34.45 PSU) of this water rather than temperature (Fig. 7). This center section also has the highest surface nitrate concentration at about 30 µmol kg^{-1} and the deepest MLD supported by the vertically homogenous density. In the DP, surface nitrate concentration is generally lower, and the nitrate concentration appears low even beneath the MLD (Fig. 6).

The center section of LB transect with high surface nitrate concentration and deep mixing is in the prolongation of northern BS current that circulated around the SSI and Elephant Islands (Fig. 1). Although its high salinity could correspond to Weddell Sea Water transported along the slope on the western side of the Powell Basin, its intermediate temperature rather supports a western origin (TWB). Physical ocean modelling supported by tidal stations suggests that tidal interaction on the shelf of the SSI arc actively mixes the water, mixing in high salinity from deeper water and homogenizing the density profile (Zhou et al., 2020). The vertical homogeneity of density remains when the water is transported downstream, allowing for the wind mixing to take over and maintain a deep mixed layer, visible in the 60.7–61.7 °S section of the LB transect. Activation energy for wind-mixing is lowered in case of lower density gradient (Pollard et al., 1973), which means that a similar wind stress will result in a deeper mixing. Surface nitrate concentration appears closely related to oceanographic circulation.

Two mechanisms may explain higher nitrate concentration in deeply mixed water: (1) quantitatively greater initial nitrate pool, due to a larger volume (or greater resupply) meaning that for an equal uptake per area unit, the concentration remains higher; and (2) lower nitrate uptake due to a limited productivity. Nitrogen isotopes can provide insight onto the latter hypothesis.

Generally, δ^{15}N of nitrate negatively correlates with its concentrations: there is a visible correspondence between low surface nitrate concentrations (Fig. 6a) and high δ^{15}N of nitrates (Fig. 6b). δ^{15}N is low (4.5 to 5 ‰) in waters deeper

https://doi.org/10.5194/egusphere-2024-3687
Preprint. Discussion started: 6 December 2024

than 125 m, where nitrate concentration exceeds 30 µmol kg^{-1}, and reaches high values of up to 6.8 ‰ near the surface in DP where nitrate concentrations are the lowest (23 µmol kg^{-1}) of these transects. This negative correlation is consistent with previous works, and reflects the isotopic fractionation during partial uptake of the available nitrate (Altabet, 2006; Lourey et al., 2003; Sigman et al., 1999). While the nitrate reservoir is not strictly isolated in summer, exchanges between surface mixed layer and subsurface waters are limited due to the density gradient preventing wind-activated mixing (Lewis et al., 1986; Pollard et al., 1973). When approximating surface waters above the MLD as a closed system, fractionation during nitrate uptake follows a Rayleigh-type isotopic distillation (Lourey et al., 2003). In the Rayleigh distillation, the $\delta^{15}N$ is linearly correlated with the logarithm of nitrate concentration (DiFiore et al., 2009; Mariotti et al., 1981). We thus quantify the isotopic effect of nitrate uptake following the linear regression on logarithmic concentration scale method (DiFiore et al., 2009; Appendix Fig. A2).

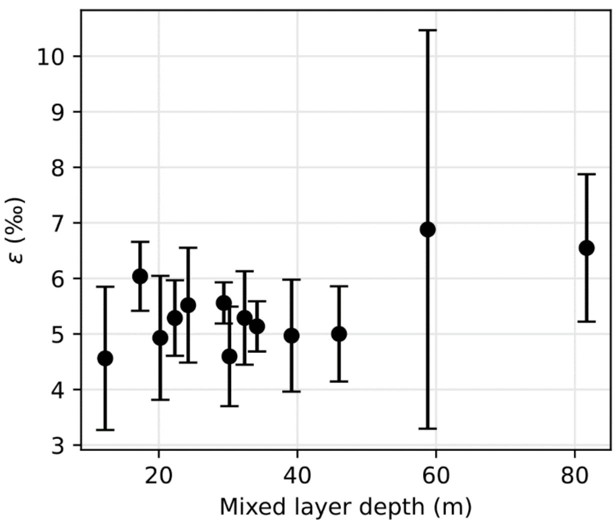

Figure 8. Nitrogen isotope effect *ε* as a function of the mixed layer depth. Error bars indicate the 95 % confidence interval for *ε* estimation.

Nitrate assimilation has been reported to imprint a nitrogen isotope effect of about 5 ‰ in SO field studies (DiFiore et al., 2009, 2010; Sigman et al., 1999). Under light limitation, the isotope effect shows notable increase, with values exceeding 8 ‰ (DiFiore et al., 2010), which is considered to be the result of continuous active pumping of nitrate to offset nitrate loss by diffusion through cell membrane, when assimilatory nitrate reduction is slowed by light-limited cellular activity (Needoba et al., 2004; Needoba and Harrison, 2004). Here, most profiles support nitrogen isotope effects ε of 5 ‰, as long as the MLD is shallower than 50 m (Fig. 8). The two profiles where the MLD is deeper, which are in the central section of LB at 61 °S and 61.7 °S, indicate slightly higher ε of 6.5 ± 1.4 ‰ and 6.9 ± 3.5 ‰, respectively. These higher ε mark light limitation in deeply mixed surface layers (DiFiore et al., 2010), and therefore support the hypothesis of lower nitrate utilization as a cause for the elevated nitrate concentration in the central section of LB. However, these ε values are lower than those previously reported for comparable MLD in the open Antarctic Zone, where sea ice is typically absent (DiFiore et al., 2010). This is likely due to stronger seasonal variability in the MLD related to the presence of seasonal sea ice in our study, suggesting that the MLD may have been shallower at the start of growth season. The data from DiFiore et al. (2010) for ocean zones with sea ice do not support ε values exceeding 5 ‰, because summer mixed layers in the Indian sector of SO are generally shallower than 50 m. This is consistent with our findings except for the two profiles with deep mixing.

https://doi.org/10.5194/egusphere-2024-3687
Preprint. Discussion started: 6 December 2024

Nitrogen recycling through heterotrophic activity may modify the isotopic repartition between organic and dissolved inorganic nitrogen (Sigman and Fripiat, 2019). Recycling of N through nitrification preferentially converts ^{14}N and may decrease the apparent ε of N uptake (DiFiore et al., 2009). In the summer, however, contribution of regenerated nitrogen to phytoplankton productivity is low, with *f*-ratio usually higher than 0.6 in the BS (Bode et al., 2002) and WS (Flynn et al., 2021), and nitrate supplied by nitrification accounts for less than 10 % of nitrate uptake (Flynn et al., 2021; Mdutyana et al., 2020). This means that more than half of summer nitrogen consumption consists of new nitrate uptake from the environment. Low regeneration rate is due to reduced heterotrophic activity in cold oceans, while light inhibits nitrification in summer. The nitrogen isotope effect ε in KARP-20 profiles is close to or higher than the reported values for ε, so they are in line with low nitrate recycling, not detectible in the nitrogen isotopes.

Despite minor changes in ε in light-limiting conditions, the relationship between nitrate depletion and $\delta^{15}N$ elevation that has been previously described in other regions of the SO (DiFiore et al., 2010; Lourey et al., 2003; Sigman et al., 1999) holds true in the ice-covered region of the Antarctic Peninsula.

4.2.2 Nitrogen isotope modelling

In this final section, we reproduce the $\delta^{15}N$ signatures of nitrate using a nitrogen isotope box-model (Yoshikawa et al., 2005) in three oceanic locations around the Antarctic Peninsula: the seasonally ice-covered part of DP (60°S, 60°W), semi-enclosed eastern BS (62°S, 55°W), and the northwestern WS (64°S, 50°W) where sea ice exits the Weddell Gyre. The model simulates a nitrogen cycle in a sea ice covered ocean, focusing on surface (0-20 m) and subsurface (20-120 m) layers, from inputs of seawater temperature, mixing depth, insolation, and nitrate concentration and its $\delta^{15}N$ at the 120 m boundary condition (Fig. 9). The model has a daily time resolution with a simulation length of one year (after 4 years spin-up), and reproduces an ideal annual cycle at equilibrium, *i.e.* repeating itself given the same forcings.

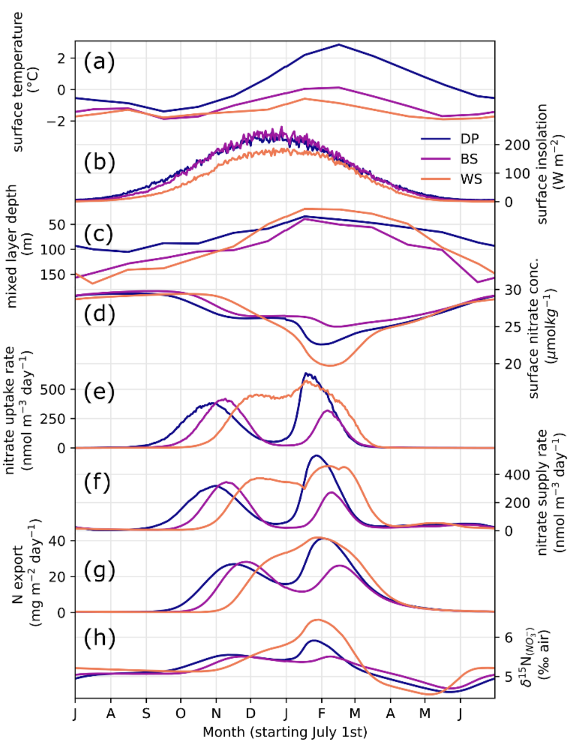

Figure 9. Seasonal variability of model forcings and results: surface water temperature (a), insolation (b), MLD (c), surface nitrate concentration (d), nitrate uptake rate in surface model box (e), nitrate supply rate from subsurface to surface (f),

https://doi.org/10.5194/egusphere-2024-3687
Preprint. Discussion started: 6 December 2024

sinking particulate N export (g), and δ^{15}N of nitrate in the surface model box (h) in three oceanic locations (DP, BS, and WS).

We first give a brief description of environmental parameters used to constrain the model. Temperature variability is strongest in the DP location (60 °S, 60 °W), which averages 1.7 °C in summer, when BS reaches a maximum of around 0°C (Fig. 9a, Fig. 10a). The temperature at the WS location is buffered by the presence of sea ice, and remains below -0.5°C year-round. Insolation is roughly similar for the three sites, although slightly lower in the WS due to the higher latitude. MLD follows the typical seasonal variability (Behera et al., 2020), shoaling in the spring and summer and deepening during autumn and winter. It is implemented indirectly in the model, regulating the exchange rates between surface and subsurface layers, rather than modifying the layer thickness in the model. The amplitude of MLD variability is greater for BS and WS, where more sea ice is present (Fig. 9c, Fig. 10d). The MLD in BS remains deeper even in summer, averaging 59 m. BS location has an intermediate temperature and yearly sea ice (Fig. 10a, 10b), but also the greatest sea ice standard deviation (Fig. 10c), used to approximate the seasonal variability of sea ice cover here. Despite greater change in sea ice cover, the summer MLD is still greater in BS location, which goes against the hypothesis of a sea ice meltwater induced summer stratification (Taylor et al., 2013), and confirms that sea ice seasonal variability is not the main control on summer MLD in this region (as discussed in Sect. 4.1).

The model simulates the N cycle in the surface ocean and its impact on δ^{15}N (Fig. 9d–h, Fig. 10e–k). For DP and BS locations, the resulting annual cycle of seawater nitrate has two peaks of nitrate uptake, corresponding to spring and summer phytoplankton blooms. This matches the two-peak chlorophyll seasonality reported for the Antarctic Circumpolar Current (Prend et al., 2022). Consequently, nitrate depletion in the surface waters increases in two steps in spring and summer, with lower minimal concentration at DP location. Although dual blooming is observed in the environment, it usually is not as clear as the idealized cycle produced by the model, with observed maxima overlapping, or double blooms not repeating every year. At the WS location, growth season is shorter due to its onset delayed by the late melting of sea ice, resulting in a single yearly maximum rate of nitrate uptake. Nevertheless, WS has a greater nitrate depletion (Fig. 10j) in the surface layer compared to the two other locations, driven by higher nutrient uptake in the strongly stratified surface ocean (Fig. 10f). The BS location with the deepest mixed layer is characterized by a lower nitrate uptake especially in the later part of summer (Fig. 9e), resulting in a lower depletion and higher concentration relative to the two other locations. δ^{15}N of nitrate (Fig. 10i) scales with the net nitrate uptake (Fig. 10f-h), with maximum ^{15}N-enrichment at WS location, and minimum at BS location. The model predicts that N export due to sinking particulate organic matter follows the same pattern (Fig. 10k).

https://doi.org/10.5194/egusphere-2024-3687
Preprint. Discussion started: 6 December 2024

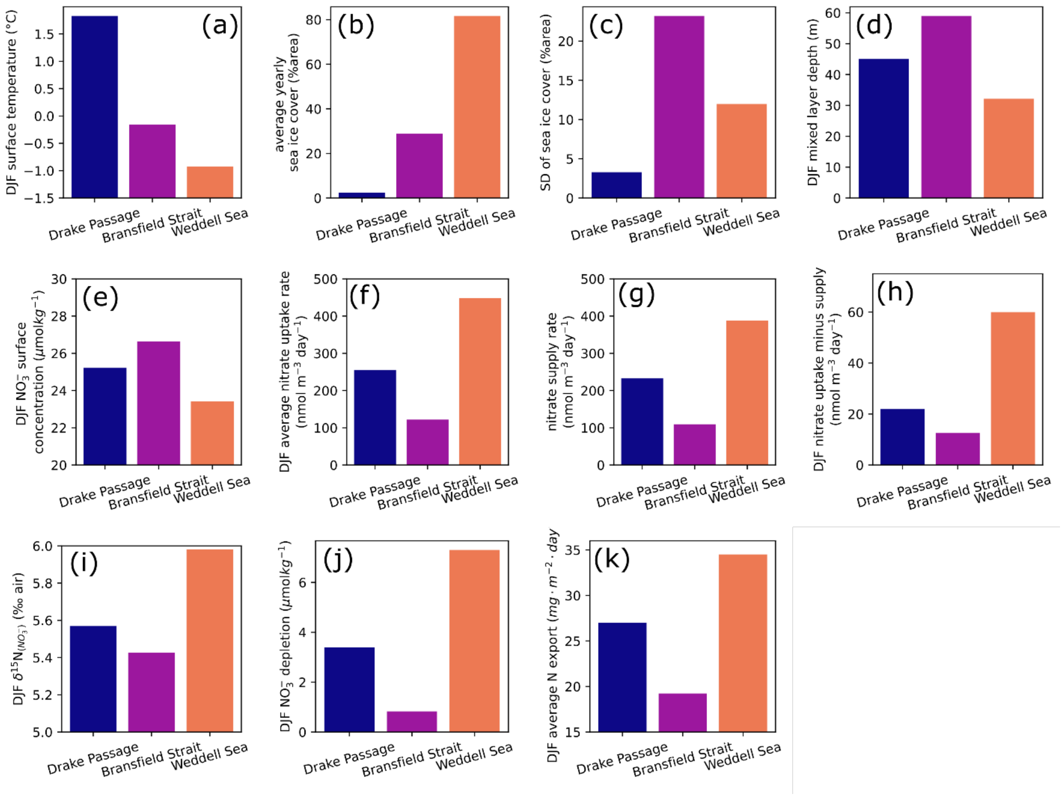

Figure 10. Summer (December, January, and February) averages of model forcings and results for (a) surface water temperature, (d) mixed layer depth, (e) surface nitrate concentration, (f) nitrate uptake rate by primary producers, (g) nitrate supply rate from subsurface to surface model layer, (h) difference between uptake and supply rates, (i) $\delta^{15}N$ of nitrate in surface water, (j) nitrate depletion in the surface water, (k) total nitrogen export in the sinking flux in three oceanic locations. Yearly sea ice parameters are given for (b) average and (c) standard deviation, used here to quantify seasonal variability. Upper row plots (a-d) are environmental forcings, with temperature (a) and mixing depth (d) forcing the model. Lower rows (e-k) describe nitrogen cycle model results.

Both in the model results and in the latitudinal transect (Sect. 4.1), it appears that the eastern BS has the lowest productivity due to its deeper mixed layer, despite intermediate temperature and sea ice seasonality. The higher surface nitrate concentration of the model for BS matches the 61–62 °S section with high surface nitrate concentration (Fig. 6), although absolute values are slightly lower in the model. Timing-wise, the model tends to predict a larger divergence of nitrate concentration at the BS location in the later part of summer (Fig. 9), but the nitrate concentration already differs in December observations, in part due to a light-limited productivity. The area of low nitrate uptake east of the SSI matches the low chlorophyll area in the climatology of surface ocean color (La et al., 2019). The location of BS point chosen for the model may not be exactly in this low chlorophyll area but closer to the Peninsula Front. However, model results should not differ because the two are characterized with a relatively deep summer mixing and similar ice cover. In addition, the eastern BS is notably characterized with a deepening of isopycnals (Frey et al., 2022; Huneke et al., 2016) and deeper chlorophyll maximum (Pereira Granja Russo et al., 2018), attesting that the MLD increases eastward, and primary producers are likely dragged to deeper waters.

In the SO, despite low temperature, a significant portion of particulate organic matter is remineralized in the water column, and nitrogen loss in surface water by sinking particles is compensated by the upwelling of nutrients, although seasonality of these fluxes is not in phase (Mdutyana et al., 2020). Here, we focused on the summer season, therefore

https://doi.org/10.5194/egusphere-2024-3687
Preprint. Discussion started: 6 December 2024

the net export of nitrogen that we report does not represent an annual flux. However, the model indicates that productivity decreases with deeper mixing, with reduced flux of sinking particles in the summer. The inferred primary productivity changes may also have implications for the carbon cycle and the biological pump.

5. Conclusions

We investigated nitrate dynamics near the Antarctic Peninsula in the Southern Ocean, to better understand environmental controls on primary productivity. We compiled measurements from different databases and new transects for a total of 394 nitrate profiles. In this region seasonally covered by sea ice, nitrate is not limiting productivity, and remains in concentrations above 20 μmol kg^{-1} at any time of the year. We evaluated the influence of sea ice on nitrate depletion in the surface water, testing the hypothesis that sea ice melting reduces surface salinity and enhances the stratification propitious to primary producers (Taylor et al., 2013). We used nitrate depletion, defined as surface concentration minus concentration in the Winter Water layer, as an indicator of nutrient uptake and net seasonal productivity. Results do not clearly point to a change in nitrate depletion in regions where sea ice duration differs. Significant nitrate depletion is mostly observed after melting, owing to favorable conditions for blooming after ice melt. However, sea ice melting is not necessarily followed by nitrate depletion. Seasonal amplitude of sea ice only marginally affects nitrate depletion and stratification, opposing the hypothesis that sea ice meltwater controls stratification at the regional scale. Diverse oceanographic controls in the water masses properties, density gradients and mixing mask the impact of sea ice on nitrate depletion when comparing a variety of locations.

Analysis of nitrate along new north-south transects in the DP and Powell basin east of the BS reveals a channel of deeply mixed waters with high surface nitrate concentration. We interpret this channel to be a remnant of actively homogenized water with tidal mixing along the SSI upstream the BS (Zhou et al., 2020). $\delta^{15}N$ of nitrate in these transects confirm the previously established relationship between nitrate drawdown and ^{15}N-enrichment in the remaining nitrate. The strong correlation between logarithm of nitrate concentration and $\delta^{15}N$ indicate that the system is well approximated by a Rayleigh distillation, with limited resupply of nitrate during phytoplankton growth. Furthermore, the higher nitrogen isotope effect estimated in the deeply mixed profiles suggests a light limitation during nitrate uptake, contributing to the lower nitrate depletion at these locations. Nitrogen isotope modeling further supports that deeper mixing in the BS induces light limitation, with lower nitrate uptake and $\delta^{15}N$ compared to both the DP and the WS. Weaker sinking particle flux in the eastern BS equates to weaker organic matter export in summer.

Strong stratification in the summer surface ocean makes nitrate depletion a seasonal-lasting feature, useful for integrating biological uptake over a growth season. However, variations in MLD makes it difficult to quantify nitrate uptake and productivity based on concentration alone, but hints towards weaker productivity in deeply mixed layer allows the use of nitrate concentration for qualitative estimates. Nitrate utilization appears tied to the MLD, which hardly depends on sea ice meltwater release. Multiple oceanographic features influence the MLD at the regional scale, with varying water masses and mixing dynamics affecting vertical density. Nonetheless, it should be noted that heavily sea-iced areas are comparatively under-sampled, and future efforts may be oriented to fill this knowledge gap.

Increasing temperatures with global climate change will likely reduce the extent of sea ice in the future. Summer stratification could shift from a salinity-based density gradient to a temperature-based density gradient. This will probably impact phytoplanktonic activity and ecosystems in a warmer surface layer with a longer ice-free season. A supposed decrease in freshwater supply in the surface ocean would tend to increase MLD inducing light limitation on phytoplanktonic productivity, but this would be counterbalanced by increased productivity in warmer waters and longer growth season. Determining which of these two effects prevails is crucial to understand future changes in the phytoplankton productivity of the high latitude Southern Ocean.

Appendix A: Station-specific profiles and isotope effect

https://doi.org/10.5194/egusphere-2024-3687
Preprint. Discussion started: 6 December 2024

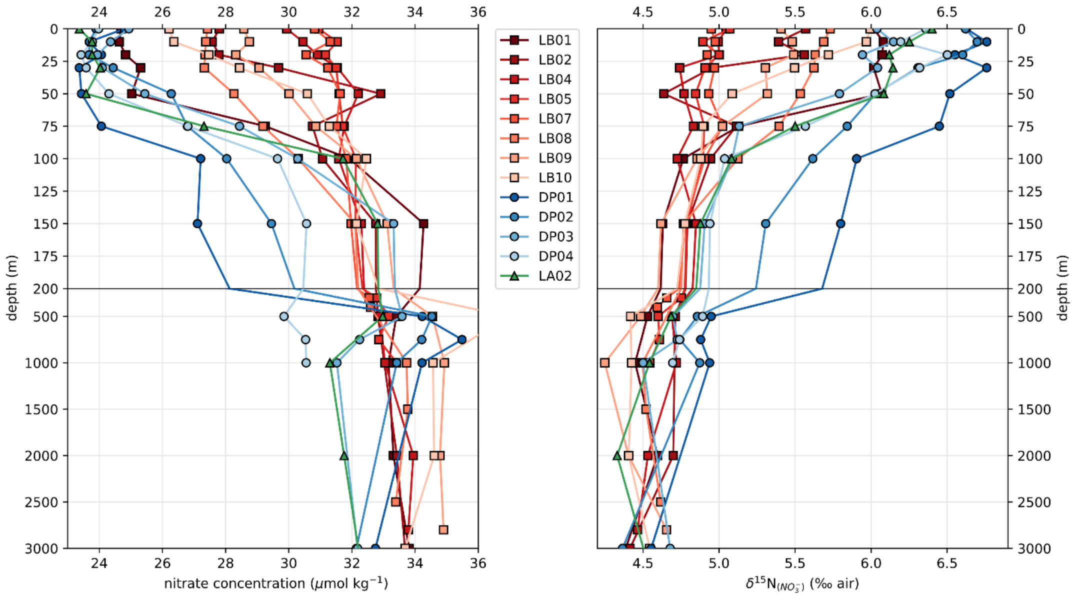

545

546 **Figure A1. Station-specific profiles of (a) nitrate concentration and (b) δ^{15}N of nitrate.**

https://doi.org/10.5194/egusphere-2024-3687
Preprint. Discussion started: 6 December 2024

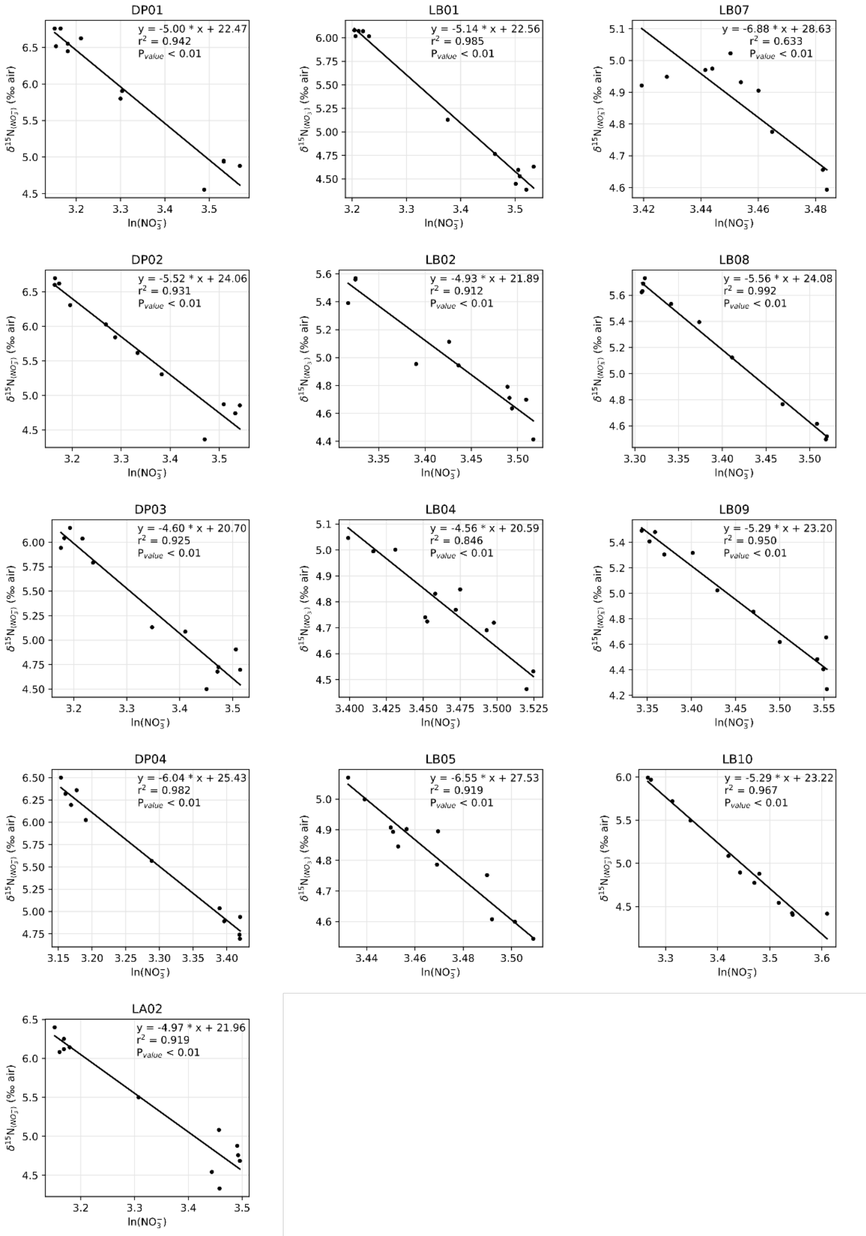

Figure A2. δ^{15}N of nitrate as a function of nitrate concentration (logarithmic scale) for each KARP-20 profile, used for estimation of nitrate isotope effect ε (opposite of the slope value, Eq. (1)).

Code availability

Python code for data processing and figure creation is available on a Zenodo repository (doi:10.5281/zenodo.14221104) for transparency and reproducibility purposes. Potential users should know that it was developed for personal use and has not been cleaned up before distribution. Nitrogen cycle model inquiries should be sent to C. Yoshikawa (yoshikawac@jamstec.go.jp).

Data availability

KARP-20 data inquiries should be addressed to B.-K. Khim (bkkhim@pusan.ac.kr), and data will be distributed after evaluation of the request. GLODAP bottle data is available for download at https://glodap.info/ [last access: November 2024]. SOCCOM float data is available for download at https://soccom.princeton.edu/float-data-single-float-profiles [last access: November 2024]. Sea ice concentration data is available for download at https://osi-saf.eumetsat.int/ https://glodap.info/ [last access: November 2024].

Sample availability

Samples from this study are not available.

Author contribution

Concept of the study, formal analysis and figure creation were conducted by APMS, as part of project co-led by FJJE and NO. The nitrogen model was developed by CY. Water samples were collected by YJ and BKK. Nitrogen data was obtained and curated by YJ, BKK, YR and DMS at Princeton university. The original manuscript prepared by APMS, YI, and CY, with revisions from BKK, NOO, YR, FJJE and NO.

Competing interests

The authors declare that they have no conflict of interest.

Acknowledgements

Float data were collected and made freely available by the Southern Ocean Carbon and Climate Observations and Modeling (SOCCOM) Project funded by the National Science Foundation, Division of Polar Programs (NSF PLR-1425989, with extension NSF OPP-1936222), and by the Global Ocean Biogeochemistry Array (GO-BGC) Project funded by the National Science Foundation, Division of Ocean Sciences (NSF OCE-1946578), supplemented by NASA, and by the International Argo Program and the NOAA programs that contribute to it. The Argo Program is part of the Global Ocean Observing System (doi:10.17882/42182, https://www.ocean-ops.org/board?t=argo). We thank the GLODAP project members who maintain and update the quality-controlled discrete sample database. The data from the EUMETSAT Satellite Application Facility on Ocean and Sea Ice used in this study are accessible through the SAF's homepage (https://osi-saf.eumetsat.int/). We are grateful to Thomas Lavergne for guidance and updates of the sea ice product. We would like to thank the members of the KARP-20 research expedition for collecting samples and making this work possible.

Financial Support

Collection and analysis of samples presented in this study were supported by Korea Institute of Marine Science & Technology funded by the Ministry of Oceans and Fisheries (RS-2023-00256330: to BKK).

References

Altabet, M. A.: Isotopic Tracers of the Marine Nitrogen Cycle: Present and Past, in: Marine Organic Matter: Biomarkers, Isotopes and DNA, edited by: Volkman, J. K., Springer, Berlin, Heidelberg, 251–293, doi:10.1007/698_2_008, 2006.

Altabet, M. A. and Francois, R.: Nitrogen isotope biogeochemistry of the Antarctic Polar Frontal Zone at 170°W, Deep Sea Research Part II: Topical Studies in Oceanography, 48, 4247–4273, doi:10.1016/S0967-0645(01)00088-1, 2001.

https://doi.org/10.5194/egusphere-2024-3687
Preprint. Discussion started: 6 December 2024

Aoyama, M.: Global certified-reference-material- or reference-material-scaled nutrient gridded dataset GND13, Earth System Science Data, 12, 487–499, doi:10.5194/essd-12-487-2020, 2020.

Ardelan, M. V., Holm-Hansen, O., Hewes, C. D., Reiss, C. S., Silva, N. S., Dulaiova, H., Steinnes, E., and Sakshaug, E.: Natural iron enrichment around the Antarctic Peninsula in the Southern Ocean, Biogeosciences, 7, 11–25, doi:10.5194/bg-7-11-2010, 2010.

Armstrong, F. A. J., Stearns, C. R., and Strickland, J. D. H.: The measurement of upwelling and subsequent biological process by means of the Technicon Autoanalyzer® and associated equipment, Deep Sea Research and Oceanographic Abstracts, 14, 381–389, doi:10.1016/0011-7471(67)90082-4, 1967.

Arrigo, K. R.: Sea ice as a habitat for primary producers, in: Sea Ice, John Wiley & Sons, Ltd, 352–369, doi:10.1002/9781118778371.ch14, 2017.

Arrigo, K. R., Worthen, D., Schnell, A., and Lizotte, M. P.: Primary production in Southern Ocean waters, Journal of Geophysical Research: Oceans, 103, 15587–15600, doi:10.1029/98JC00930, 1998.

Arrigo, K. R., van Dijken, G. L., and Bushinsky, S.: Primary production in the Southern Ocean, 1997–2006, Journal of Geophysical Research: Oceans, 113, C08004, doi:10.1029/2007JC004551, 2008.

Arteaga, L. A., Boss, E., Behrenfeld, M. J., Westberry, T. K., and Sarmiento, J. L.: Seasonal modulation of phytoplankton biomass in the Southern Ocean, Nat Commun, 11, 5364, doi:10.1038/s41467-020-19157-2, 2020.

Behera, N., Swain, D., and Sil, S.: Effect of Antarctic sea ice on chlorophyll concentration in the Southern Ocean, Deep Sea Research Part II: Topical Studies in Oceanography, 178, 104853, doi:10.1016/j.dsr2.2020.104853, 2020.

Bélanger, S., Ehn, J. K., and Babin, M.: Impact of sea ice on the retrieval of water-leaving reflectance, chlorophyll a concentration and inherent optical properties from satellite ocean color data, Remote Sensing of Environment, 111, 51–68, doi:10.1016/j.rse.2007.03.013, 2007.

Bode, A., Castro, C. G., Doval, M. D., and Varela, M.: New and regenerated production and ammonium regeneration in the western Bransfield Strait region (Antarctica) during phytoplankton bloom conditions in summer, Deep Sea Research Part II: Topical Studies in Oceanography, 49, 787–804, doi:10.1016/S0967-0645(01)00124-2, 2002.

de Boyer Montégut, C., Madec, G., Fischer, A. S., Lazar, A., and Iudicone, D.: Mixed layer depth over the global ocean: An examination of profile data and a profile-based climatology, Journal of Geophysical Research: Oceans, 109, C12003, doi:10.1029/2004JC002378, 2004.

Braman, R. S. and Hendrix, S. A.: Nanogram nitrite and nitrate determination in environmental and biological materials by vanadium(III) reduction with chemiluminescence detection, Anal. Chem., 61, 2715–2718, doi:10.1021/ac00199a007, 1989.

Castro, C. G., Ríos, A. F., Doval, M. D., and Pérez, F. F.: Nutrient utilisation and chlorophyll distribution in the Atlantic sector of the Southern Ocean during Austral summer 1995–96, Deep Sea Research Part II: Topical Studies in Oceanography, 49, 623–641, doi:10.1016/S0967-0645(01)00115-1, 2002.

Codispoti, L. A., Kelly, V., Thessen, A., Matrai, P., Suttles, S., Hill, V., Steele, M., and Light, B.: Synthesis of primary production in the Arctic Ocean: III. Nitrate and phosphate based estimates of net community production, Progress in Oceanography, 110, 126–150, doi:10.1016/j.pocean.2012.11.006, 2013.

DeVries, T., Primeau, F., and Deutsch, C.: The sequestration efficiency of the biological pump, Geophysical Research Letters, 39, L13601, doi:10.1029/2012GL051963, 2012.

https://doi.org/10.5194/egusphere-2024-3687
Preprint. Discussion started: 6 December 2024

DiFiore, P. J., Sigman, D. M., and Dunbar, R. B.: Upper ocean nitrogen fluxes in the Polar Antarctic Zone: Constraints from the nitrogen and oxygen isotopes of nitrate, Geochemistry, Geophysics, Geosystems, 10, Q11016, doi:10.1029/2009GC002468, 2009.

DiFiore, P. J., Sigman, D. M., Karsh, K. L., Trull, T. W., Dunbar, R. B., and Robinson, R. S.: Poleward decrease in the isotope effect of nitrate assimilation across the Southern Ocean, Geophysical Research Letters, 37, L17601, doi:10.1029/2010GL044090, 2010.

Fahrbach, E.: Cruise Report for R/V Polarstern Expedition 06AQANTX_7 on WOCE section SR04, CLIVAR and Carbon Hydrographic Data Office, https://cchdo.ucsd.edu/cruise/06AQANTX_7, 1993.

Fan, T., Deser, C., and Schneider, D. P.: Recent Antarctic sea ice trends in the context of Southern Ocean surface climate variations since 1950, Geophysical Research Letters, 41, 2419–2426, doi:10.1002/2014GL059239, 2014.

Flynn, R. F., Bornman, T. G., Burger, J. M., Smith, S., Spence, K. A. M., and Fawcett, S. E.: Summertime productivity and carbon export potential in the Weddell Sea, with a focus on the waters adjacent to Larsen C Ice Shelf, Biogeosciences, 18, 6031–6059, doi:10.5194/bg-18-6031-2021, 2021.

Frants, M., Gille, S. T., Hatta, M., Hiscock, W. T., Kahru, M., Measures, C. I., Greg Mitchell, B., and Zhou, M.: Analysis of horizontal and vertical processes contributing to natural iron supply in the mixed layer in southern Drake Passage, Deep Sea Research Part II: Topical Studies in Oceanography, 90, 68–76, doi:10.1016/j.dsr2.2012.06.001, 2013.

Frey, D. I., Krechik, V. A., Morozov, E. G., Drozd, I. D., Gordey, A. S., Latushkin, A. A., Mekhova, O. S., Mukhametianov, R. Z., Murzina, S. A., Ostroumova, S. A., Ponomarev, V. I., Salyuk, P. A., Smirnova, D. A., Shutov, S. A., and Zuev, O. A.: Water Exchange between Deep Basins of the Bransfield Strait, Water, 14, 3193, doi:10.3390/w14203193, 2022.

Fripiat, F., Sigman, D. M., Fawcett, S. E., Rafter, P. A., Weigand, M. A., and Tison, J.-L.: New insights into sea ice nitrogen biogeochemical dynamics from the nitrogen isotopes, Global Biogeochemical Cycles, 28, 115–130, doi:10.1002/2013GB004729, 2014.

Fripiat, F., Elskens, M., Trull, T. W., Blain, S., Cavagna, A.-J., Fernandez, C., Fonseca-Batista, D., Planchon, F., Raimbault, P., Roukaerts, A., and Dehairs, F.: Significant mixed layer nitrification in a natural iron-fertilized bloom of the Southern Ocean, Global Biogeochemical Cycles, 29, 1929–1943, doi:10.1002/2014GB005051, 2015.

Garcia, H. E., Boyer, T. P., Baranova, O. K., Locarnini, R. A., Mishonov, A. V., Grodsky, A., Paver, C. R., Weathers, K. W., Smolyar, I. V., Reagan, J. R., Seidov, D., and Zweng, M. M.: World Ocean Atlas 2018 [data set], https://www.ncei.noaa.gov/data/oceans/woa/WOA18/, 2019. [Accessed July 2023]

Goeyens, L., Tréguer, P., Baumann, M. E. M., Baeyens, W., and Dehairs, F.: The leading role of ammonium in the nitrogen uptake regime of Southern Ocean marginal ice zones, Journal of Marine Systems, 6, 345–361, doi:10.1016/0924-7963(94)00033-8, 1995.

Gonçalves-Araujo, R., De Souza, M. S., Tavano, V. M., and Garcia, C. A. E.: Influence of oceanographic features on spatial and interannual variability of phytoplankton in the Bransfield Strait, Antarctica, Journal of Marine Systems, 142, 1–15, doi:10.1016/j.jmarsys.2014.09.007, 2015.

Gordon, A. L., Mensch, M., Zhaoqian, D., Smethie, W. M., and de Bettencourt, J.: Deep and bottom water of the Bransfield Strait eastern and central basins, J. Geophys. Res., 105, 11337–11346, doi:10.1029/2000JC900030, 2000.

Gruber, N., Gloor, M., Mikaloff Fletcher, S. E., Doney, S. C., Dutkiewicz, S., Follows, M. J., Gerber, M., Jacobson, A. R., Joos, F., Lindsay, K., Menemenlis, D., Mouchet, A., Müller, S. A., Sarmiento, J. L., and Takahashi, T.: Oceanic sources, sinks, and transport of atmospheric CO2, Global Biogeochemical Cycles, 23, GB1005, doi:10.1029/2008GB003349, 2009.

https://doi.org/10.5194/egusphere-2024-3687
Preprint. Discussion started: 6 December 2024

Hatta, M., Measures, C. I., Selph, K. E., Zhou, M., and Hiscock, W. T.: Iron fluxes from the shelf regions near the South Shetland Islands in the Drake Passage during the austral-winter 2006, Deep Sea Research Part II: Topical Studies in Oceanography, 90, 89–101, doi:10.1016/j.dsr2.2012.11.003, 2013.

Huang, Y. and Fassbender, A. J.: Biological Production of Distinct Carbon Pools Drives Particle Export Efficiency in the Southern Ocean, Geophysical Research Letters, 51, e2023GL107511, doi:10.1029/2023GL107511, 2024.

Huneke, W. G. C., Huhn, O., and Schröeder, M.: Water masses in the Bransfield Strait and adjacent seas, austral summer 2013, Polar Biol, 39, 789–798, doi:10.1007/s00300-016-1936-8, 2016.

Jiang, M., Measures, C. I., Barbeau, K. A., Charette, M. A., Gille, S. T., Hatta, M., Kahru, M., Mitchell, B. G., Naveira Garabato, A. C., Reiss, C., Selph, K., and Zhou, M.: Fe sources and transport from the Antarctic Peninsula shelf to the southern Scotia Sea, Deep Sea Research Part I: Oceanographic Research Papers, 150, 103060, doi:10.1016/j.dsr.2019.06.006, 2019.

Johnson, K. S. and Coletti, L. J.: In situ ultraviolet spectrophotometry for high resolution and long-term monitoring of nitrate, bromide and bisulfide in the ocean, Deep Sea Research Part I: Oceanographic Research Papers, 49, 1291–1305, doi:10.1016/S0967-0637(02)00020-1, 2002.

Johnson, K. S., Coletti, L. J., Jannasch, H. W., Sakamoto, C. M., Swift, D. D., and Riser, S. C.: Long-Term Nitrate Measurements in the Ocean Using the in situ Ultraviolet Spectrophotometer: Sensor Integration into the APEX Profiling Float, Journal of Atmospheric and Oceanic Technology, 30, 1854–1866, doi:10.1175/JTECH-D-12-00221.1, 2013.

Johnson, K. S., Plant, J. N., Coletti, L. J., Jannasch, H. W., Sakamoto, C. M., Riser, S. C., Swift, D. D., Williams, N. L., Boss, E., Haëntjens, N., Talley, L. D., and Sarmiento, J. L.: Biogeochemical sensor performance in the SOCCOM profiling float array, Journal of Geophysical Research: Oceans, 122, 6416–6436, doi:10.1002/2017JC012838, 2017.

Jones, J. M., Gille, S. T., Goosse, H., Abram, N. J., Canziani, P. O., Charman, D. J., Clem, K. R., Crosta, X., de Lavergne, C., Eisenman, I., England, M. H., Fogt, R. L., Frankcombe, L. M., Marshall, G. J., Masson-Delmotte, V., Morrison, A. K., Orsi, A. J., Raphael, M. N., Renwick, J. A., Schneider, D. P., Simpkins, G. R., Steig, E. J., Stenni, B., Swingedouw, D., and Vance, T. R.: Assessing recent trends in high-latitude Southern Hemisphere surface climate, Nature Clim Change, 6, 917–926, doi:10.1038/nclimate3103, 2016.

Kalnay, E., Kanamitsu, M., Kistler, R., Collins, W., Deaven, D., Gandin, L., Iredell, M., Saha, S., White, G., Woollen, J., Zhu, Y., Chelliah, M., Ebisuzaki, W., Higgins, W., Janowiak, J., Mo, K. C., Ropelewski, C., Wang, J., Leetmaa, A., Reynolds, R., Jenne, R., and Joseph, D.: The NCEP/NCAR 40-Year Reanalysis Project, Bulletin of the American Meteorological Society, 77, 437–472, doi:10.1175/1520-0477(1996)077<0437:TNYRP>2.0.CO;2, 1996.

Key, R. M., Olsen, A., van Heuven, S., Lauvset, S. K., Velo, A., Lin, X., Schirnick, C., Kozyr, A., Tanhua, T., Hoppema, M., Jutterström, S., Steinfeldt, R., Jeansson, E., Ishii, M., Perez, F. F., and Suzuki, T.: Global Ocean Data Analysis Project, Version 2 (GLODAPv2), Ornl/Cdiac-162, Ndp-093, 8:297–323, doi:doi:10.3334/CDIAC/OTG.NDP093_GLODAPv2, 2015.

Kwok, R. and Kacimi, S.: Three years of sea ice freeboard, snow depth, and ice thickness of the Weddell Sea from Operation IceBridge and CryoSat-2, The Cryosphere, 12, 2789–2801, doi:10.5194/tc-12-2789-2018, 2018.

La, H. S., Park, K., Chae, J. Y., Park, T., and Park, J.: Climatic factors and their robust evidences controlling phytoplankton biomass in the Bransfield Strait, Terr. Atmos. Ocean. Sci., 30, 821–830, doi:10.3319/TAO.2019.04.30.01, 2019.

Lauvset, S. K., Lange, N., Tanhua, T., Bittig, H. C., Olsen, A., Kozyr, A., Alin, S., Álvarez, M., Azetsu-Scott, K., Barbero, L., Becker, S., Brown, P. J., Carter, B. R., da Cunha, L. C., Feely, R. A., Hoppema, M., Humphreys, M. P., Ishii, M., Jeansson, E., Jiang, L.-Q., Jones, S. D., Lo Monaco, C., Murata, A., Müller, J. D., Pérez, F. F., Pfeil, B., Schirnick, C., Steinfeldt, R., Suzuki, T., Tilbrook, B., Ulfsbo, A., Velo, A., Woosley, R. J., and Key, R. M.:

GLODAPv2.2022: the latest version of the global interior ocean biogeochemical data product, Earth System Science Data, 14, 5543–5572, doi:10.5194/essd-14-5543-2022, 2022.

Lavergne, T., Sørensen, A. M., Kern, S., Tonboe, R., Notz, D., Aaboe, S., Bell, L., Dybkjær, G., Eastwood, S., Gabarro, C., Heygster, G., Killie, M. A., Brandt Kreiner, M., Lavelle, J., Saldo, R., Sandven, S., and Pedersen, L. T.: Version 2 of the EUMETSAT OSI SAF and ESA CCI sea-ice concentration climate data records, The Cryosphere, 13, 49–78, doi:10.5194/tc-13-49-2019, 2019.

Lavergne, T., Sørensen, A., Tonboe, R., Strong, C., Kreiner, M., Saldo, R., Birkedal, A., Baordo, F., Rusin, J., Aspenes, T., and Eastwood, S.: Monitoring of Sea Ice Concentration, Area, and Extent in the polar regions : 40+ years of data from EUMETSAT OSI SAF and ESA CCI, IAF Global Space Conference on Climate Change (GLOC 2023), Oslo, Norway, 23-25 May 2023, GLOC-2023,T,1,7,x75079, doi:10.5281/zenodo.10014534, 2023.

Lewis, M. R., Hebert, D., Harrison, W. G., Platt, T., and Oakey, N. S.: Vertical Nitrate Fluxes in the Oligotrophic Ocean, Science, 234, 870–873, doi:10.1126/science.234.4778.870, 1986.

Lourey, M. J., Trull, T. W., and Sigman, D. M.: Sensitivity of $\delta^{15}N$ of nitrate, surface suspended and deep sinking particulate nitrogen to seasonal nitrate depletion in the Southern Ocean, Global Biogeochem. Cycles, 17, 1081, doi:10.1029/2002GB001973, 2003.

Franck, V. M., Brzezinski, M. A., Coale, K. H., and Nelson, D. M.: Iron and silicic acid concentrations regulate Si uptake north and south of the Polar Frontal Zone in the Pacific Sector of the Southern Ocean, Deep Sea Research Part II: Topical Studies in Oceanography, 47, 3315–3338, doi:10.1016/S0967-0645(00)00070-9, 2000.

MacIntyre, G., Plache, B., Lewis, M. R., Andrea, J., Feener, S., McLean, S. D., Johnson, K. S., Coletti, L. J., and Jannasch, H. W.: ISUS/SUNA nitrate measurements in networked ocean observing systems, in: OCEANS 2009, OCEANS 2009, Biloxi, MS, 1–7, doi:10.23919/OCEANS.2009.5422251, 2009.

Mariotti, A., Germon, J. C., Hubert, P., Kaiser, P., Letolle, R., Tardieux, A., and Tardieux, P.: Experimental determination of nitrogen kinetic isotope fractionation: Some principles; illustration for the denitrification and nitrification processes, Plant Soil, 62, 413–430, doi:10.1007/BF02374138, 1981.

Maurer, T. L., Plant, J. N., and Johnson, K. S.: Delayed-Mode Quality Control of Oxygen, Nitrate, and pH Data on SOCCOM Biogeochemical Profiling Floats, Front. Mar. Sci., 8, 683207, doi:10.3389/fmars.2021.683207, 2021.

Mdutyana, M., Thomalla, S. J., Philibert, R., Ward, B. B., and Fawcett, S. E.: The Seasonal Cycle of Nitrogen Uptake and Nitrification in the Atlantic Sector of the Southern Ocean, Global Biogeochemical Cycles, 34, e2019GB006363, doi:10.1029/2019GB006363, 2020.

Measures, C. I., Brown, M. T., Selph, K. E., Apprill, A., Zhou, M., Hatta, M., and Hiscock, W. T.: The influence of shelf processes in delivering dissolved iron to the HNLC waters of the Drake Passage, Antarctica, Deep Sea Research Part II: Topical Studies in Oceanography, 90, 77–88, doi:10.1016/j.dsr2.2012.11.004, 2013.

Mengesha, S., Dehairs, F., Fiala, M., Elskens, M., and Goeyens, L.: Seasonal variation of phytoplankton community structure and nitrogen uptake regime in the Indian Sector of the Southern Ocean, Polar Biol, 20, 259–272, doi:10.1007/s003000050302, 1998.

Moffat, C. and Meredith, M.: Shelf–ocean exchange and hydrography west of the Antarctic Peninsula: a review, Phil. Trans. R. Soc. A., 376, 20170164, doi:10.1098/rsta.2017.0164, 2018.

Moline, M. and Prézelin, B.: Long-term monitoring and analyses of physical factors regulating variability in coastal Antarctic phytoplankton biomass, in situ productivity and taxonomic composition over subseasonal, seasonal and interannual time scales, Mar. Ecol. Prog. Ser., 145, 143–160, doi:10.3354/meps145143, 1996.

https://doi.org/10.5194/egusphere-2024-3687
Preprint. Discussion started: 6 December 2024

Moore, J. K., Doney, S. C., Glover, D. M., and Fung, I. Y.: Iron cycling and nutrient-limitation patterns in surface waters of the World Ocean, 49, 463-507, doi:10.1016/S0967-0645(01)00109-6, 2002.

Moreau, S., Mostajir, B., Bélanger, S., Schloss, I. R., Vancoppenolle, M., Demers, S., and Ferreyra, G. A.: Climate change enhances primary production in the western Antarctic Peninsula, Global Change Biology, 21, 2191–2205, doi:10.1111/gcb.12878, 2015.

Moreau, S., Boyd, P. W., and Strutton, P. G.: Remote assessment of the fate of phytoplankton in the Southern Ocean sea-ice zone, Nat Commun, 11, 3108, doi:10.1038/s41467-020-16931-0, 2020.

Needoba, J. A. and Harrison, P. J.: INFLUENCE OF LOW LIGHT AND A LIGHT: DARK CYCLE ON NO_3^- UPTAKE, INTRACELLULAR NO_3^-, AND NITROGEN ISOTOPE FRACTIONATION BY MARINE PHYTOPLANKTON, Journal of Phycology, 40, 505–516, doi:10.1111/j.1529-8817.2004.03171.x, 2004.

Needoba, J. A., Sigman, D. M., and Harrison, P. J.: THE MECHANISM OF ISOTOPE FRACTIONATION DURING ALGAL NITRATE ASSIMILATION AS ILLUMINATED BY THE $^{15}N/^{14}N$ OF INTRACELLULAR NITRATE, Journal of Phycology, 40, 517–522, doi:10.1111/j.1529-8817.2004.03172.x, 2004.

NOAA National Centers for Environmental Information: ETOPO 2022 15 Arc-Second Global Relief Model [data set], doi:10.25921/fd45-gt74, 2022. [Accessed 2023-05-08]

Ohkouchi, N. and Takano, Y.: Organic Nitrogen: Sources, Fates, and Chemistry, in: Treatise on Geochemistry, vol. 12, edited by: Holland, H. D. and Turekian, K. K., Elsevier, 251–289, doi:10.1016/B978-0-08-095975-7.01015-9, 2014.

Olsen, A., Key, R. M., van Heuven, S., Lauvset, S. K., Velo, A., Lin, X., Schirnick, C., Kozyr, A., Tanhua, T., Hoppema, M., Jutterström, S., Steinfeldt, R., Jeansson, E., Ishii, M., Pérez, F. F., and Suzuki, T.: The Global Ocean Data Analysis Project version 2 (GLODAPv2) – an internally consistent data product for the world ocean, Earth System Science Data, 8, 297–323, doi:10.5194/essd-8-297-2016, 2016.

OSI SAF: Global Sea Ice Concentration Climate Data Record v3.0 - Multimission, EUMETSAT SAF on Ocean and Sea Ice [data set], doi:10.15770/EUM_SAF_OSI_0013, 2022a. [Accessed 2023-09-07]

OSI SAF: Global Sea Ice Concentration Interim Climate Data Record Release 3 - DMSP, EUMETSAT SAF on Ocean and Sea Ice [data set], doi:10.15770/EUM_SAF_OSI_0014, 2022b. [Accessed 2023-09-07]

Parkinson, C. L. and Cavalieri, D. J.: Antarctic sea ice variability and trends, 1979–2010, The Cryosphere, 6, 871–880, doi:10.5194/tc-6-871-2012, 2012.

Pellichero, V., Sallée, J.-B., Schmidtko, S., Roquet, F., and Charrassin, J.-B.: The ocean mixed layer under Southern Ocean sea-ice: Seasonal cycle and forcing, Journal of Geophysical Research: Oceans, 122, 1608–1633, doi:10.1002/2016JC011970, 2017.

Pollard, R. T., Rhines, P. B., and Thompson, R. O. R. Y.: The deepening of the wind-Mixed layer, Geophysical Fluid Dynamics, 4, 381–404, doi:10.1080/03091927208236105, 1973.

Prend, C. J., Keerthi, M. G., Lévy, M., Aumont, O., Gille, S. T., and Talley, L. D.: Sub-Seasonal Forcing Drives Year-To-Year Variations of Southern Ocean Primary Productivity, Global Biogeochemical Cycles, 36, e2022GB007329, doi:10.1029/2022GB007329, 2022.

Russo, A. D.'A. P. G., de Souza, M. S., Borges Mendes, C. R., Maria Tavano, V., and Eiras Garcia, C. A.: Spatial variability of photophysiology and primary production rates of the phytoplankton communities across the western Antarctic Peninsula in late summer 2013, Deep Sea Research Part II: Topical Studies in Oceanography, 149, 99–110, doi:10.1016/j.dsr2.2017.09.021, 2018.

https://doi.org/10.5194/egusphere-2024-3687
Preprint. Discussion started: 6 December 2024

Sabine, C. L., Feely, R. A., Gruber, N., Key, R. M., Lee, K., Bullister, J. L., Wanninkhof, R., Wong, C. S., Wallace, D. W. R., Tilbrook, B., Millero, F. J., Peng, T.-H., Kozyr, A., Ono, T., and Rios, A. F.: The Oceanic Sink for Anthropogenic CO2, Science, 305, 367–371, doi:10.1126/science.1097403, 2004.

Sallée, J. B., Speer, K. G., and Rintoul, S. R.: Zonally asymmetric response of the Southern Ocean mixed-layer depth to the Southern Annular Mode, Nature Geosci, 3, 273–279, doi:10.1038/ngeo812, 2010.

Sangrà, P., Gordo, C., Hernández-Arencibia, M., Marrero-Díaz, A., Rodríguez-Santana, A., Stegner, A., Martínez-Marrero, A., Pelegrí, J. L., and Pichon, T.: The Bransfield current system, Deep Sea Research Part I: Oceanographic Research Papers, 58, 390–402, doi:10.1016/j.dsr.2011.01.011, 2011.

Savidge, G., Priddle, J., Gilpin, L. C., Bathmann, U., Murphy, E. J., Owens, N. J. P., Pollard, R. T., Turner, D. R., Veth, C., and Boyd, P.: An assessment of the role of the marginal ice zone in the carbon cycle of the Southern Ocean, Antarctic Science, 8, 349–358, doi:10.1017/S0954102096000521, 1996.

Sherrell, R. M., Annett, A. L., Fitzsimmons, J. N., Roccanova, V. J., and Meredith, M. P.: A 'shallow bathtub ring' of local sedimentary iron input maintains the Palmer Deep biological hotspot on the West Antarctic Peninsula shelf, Philosophical Transactions of the Royal Society A: Mathematical, Physical and Engineering Sciences, 376, 20170171, doi:10.1098/rsta.2017.0171, 2018.

Sigman, D. M. and Fripiat, F.: Nitrogen Isotopes in the Ocean, in: Encyclopedia of Ocean Sciences, vol. 1, edited by: Cochran, J. K., Bokuniewicz, H. J., and Yager, P. L., Elsevier, 263–278, doi:10.1016/B978-0-12-409548-9.11605-7, 2019.

Sigman, D. M., Altabet, M. A., McCorkle, D. C., Francois, R., and Fischer, G.: The δ^{15}N of nitrate in the southern ocean: Consumption of nitrate in surface waters, Global Biogeochem. Cycles, 13, 1149–1166, doi:10.1029/1999GB900038, 1999.

Sigman, D. M., Casciotti, K. L., Andreani, M., Barford, C., Galanter, M., and Böhlke, J. K.: A Bacterial Method for the Nitrogen Isotopic Analysis of Nitrate in Seawater and Freshwater, Anal. Chem., 73, 4145–4153, doi:10.1021/ac010088e, 2001.

Smart, S. M., Fawcett, S. E., Thomalla, S. J., Weigand, M. A., Reason, C. J. C., and Sigman, D. M.: Isotopic evidence for nitrification in the Antarctic winter mixed layer, Global Biogeochemical Cycles, 29, 427–445, doi:10.1002/2014GB005013, 2015.

Smith, W. O. and Nelson, D. M.: Importance of Ice Edge Phytoplankton Production in the Southern Ocean, BioScience, 36, 251–257, doi:10.2307/1310215, 1986.

Soppa, M., Völker, C., and Bracher, A.: Diatom Phenology in the Southern Ocean: Mean Patterns, Trends and the Role of Climate Oscillations, Remote Sensing, 8, 420, doi:10.3390/rs8050420, 2016.

Taylor, M. H., Losch, M., and Bracher, A.: On the drivers of phytoplankton blooms in the Antarctic marginal ice zone: A modeling approach, Journal of Geophysical Research: Oceans, 118, 63–75, doi:10.1029/2012JC008418, 2013.

Thomas, R. K., Fawcett, S. E., Forrer, H. J., Robinson, C. M., and Knapp, A. N.: Estimates of the Isotope Effect for Nitrate Assimilation in the Indian Sector of the Southern Ocean, Journal of Geophysical Research: Oceans, 129, e2023JC020830, doi:10.1029/2023JC020830, 2024.

Thompson, A. F., Heywood, K. J., Thorpe, S. E., Renner, A. H. H., and Trasviña, A.: Surface Circulation at the Tip of the Antarctic Peninsula from Drifters, Journal of Physical Oceanography, 39, 3–26, doi:10.1175/2008JPO3995.1, 2009.

Uotila, P., Holland, P. R., Vihma, T., Marsland, S. J., and Kimura, N.: Is realistic Antarctic sea-ice extent in climate models the result of excessive ice drift?, Ocean Modelling, 79, 33–42, doi:10.1016/j.ocemod.2014.04.004, 2014.

https://doi.org/10.5194/egusphere-2024-3687
Preprint. Discussion started: 6 December 2024

Vorrath, M.-E., Müller, J., Rebolledo, L., Cárdenas, P., Shi, X., Esper, O., Opel, T., Geibert, W., Muñoz, P., Haas, C., Kuhn, G., Lange, C. B., Lohmann, G., and Mollenhauer, G.: Sea ice dynamics in the Bransfield Strait, Antarctic Peninsula, during the past 240 years: a multi-proxy intercomparison study, Climate of the Past, 16, 2459–2483, doi:10.5194/cp-16-2459-2020, 2020.

Wang, W.-L., Fu, W., Le Moigne, F. A. C., Letscher, R. T., Liu, Y., Tang, J.-M., and Primeau, F. W.: Biological carbon pump estimate based on multidecadal hydrographic data, Nature, 624, 579–585, doi:10.1038/s41586-023-06772-4, 2023.

Wang, X. and Wu, Z.: Variability in Polar Sea Ice (1989–2018), IEEE Geosci. Remote Sensing Lett., 18, 1520–1524, doi:10.1109/LGRS.2020.3004257, 2021.

Wanninkhof, R., Johnson, K., Williams, N., Sarmiento, J., Riser, S., Briggs, E., Bushinsky, S., Carter, B., Dickson, A., Feely, R., Gray, A., Juranek, L., Key, R., Talley, L., Russel, J., and Verdy, A.: An Evaluation of pH and NO_3 Sensor Data from SOCCOM Floats and their Utilization to Develop Ocean Inorganic Carbon Products, Marine Science Faculty Publications, 1342, https://digitalcommons.usf.edu/msc_facpub/1342, 2016.

Waser, N., Yin, K., Yu, Z., Tada, K., Harrison, P., Turpin, D., and Calvert, S.: Nitrogen isotope fractionation during nitrate, ammonium and urea uptake by marine diatoms and coccolithophores under various conditions of N availability, Mar. Ecol. Prog. Ser., 169, 29–41, doi:10.3354/meps169029, 1998.

Williams, G., Maksym, T., Wilkinson, J., Kunz, C., Murphy, C., Kimball, P., and Singh, H.: Thick and deformed Antarctic sea ice mapped with autonomous underwater vehicles, Nature Geosci, 8, 61–67, doi:10.1038/ngeo2299, 2015.

Yoshikawa, C., Yamanaka, Y., and Nakatsuka, T.: An Ecosystem Model Including Nitrogen Isotopes: Perspectives on a Study of the Marine Nitrogen Cycle, J Oceanogr, 61, 921–942, doi:10.1007/s10872-006-0010-5, 2005.

Yoshikawa, C., Ogawa, N. O., Chikaraishi, Y., Makabe, A., Matsui, Y., Sasai, Y., Wakita, M., Honda, M. C., Mino, Y., Aita, M. N., Fujiki, T., Nunoura, T., Harada, N., and Ohkouchi, N.: Nitrogen Isotopes of Sinking Particles Reveal the Seasonal Transition of the Nitrogen Source for Phytoplankton, Geophysical Research Letters, 49, e2022GL098670, doi:10.1029/2022GL098670, 2022.

Yoshikawa, C., Shigemitsu, M., Yamamoto, A., Oka, A., and Ohkouchi, N.: A nitrogen isoscape of phytoplankton in the western North Pacific created with a marine nitrogen isotope model, Front. Mar. Sci., 11, 1294608, doi:10.3389/fmars.2024.1294608, 2024.

Zehr, J. P. and Capone, D. G.: Biogeography of N2 Fixation in the Surface Ocean, in: Marine Nitrogen Fixation, Springer, Cham, 117–141, doi:10.1007/978-3-030-67746-6_7, 2021.

Zhou, X., Zhu, G., and Hu, S.: Influence of tides on mass transport in the Bransfield Strait and the adjacent areas, Antarctic, Polar Science, 23, 100506, doi:10.1016/j.polar.2020.100506, 2020.